



HO_x radical chemistry in oxidation flow reactors with low-pressure mercury lamps systematically examined by modeling

Z. Peng^{1,2}, D. A. Day^{1,2}, H. Stark^{1,2,3}, R. Li^{1,4,5}, J. Lee-Taylor^{1,2}, B. B. Palm^{1,2}, W. H. Brune⁶, and J. L. Jimenez^{1,2}

¹Cooperative Institute for Research in Environmental Sciences, University of Colorado, Boulder, CO 80309, USA

²Department of Chemistry and Biochemistry, University of Colorado, Boulder, CO 80309, USA

³Aerodyne Research, Inc., Billerica, MA 01821, USA

⁴Department of Atmospheric and Oceanic Sciences, University of Colorado, Boulder, CO 80309, USA

⁵Chemical Sciences Division, Earth System Research Laboratory, National Oceanic and Atmospheric Administration, Boulder, CO 80305, USA

⁶Department of Meteorology, Pennsylvania State University, University Park, Pennsylvania, PA 16802, USA

Correspondence to: J. L. Jimenez (jose.jimenez@colorado.edu)

Received: 4 March 2015 – Published in Atmos. Meas. Tech. Discuss.: 20 April 2015

Revised: 30 October 2015 – Accepted: 8 November 2015 – Published: 20 November 2015

Abstract. Oxidation flow reactors (OFRs) using OH produced from low-pressure Hg lamps at 254 nm (OFR254) or both 185 and 254 nm (OFR185) are commonly used in atmospheric chemistry and other fields. OFR254 requires the addition of externally formed O₃ since OH is formed from O₃ photolysis, while OFR185 does not since O₂ can be photolyzed to produce O₃, and OH can also be formed from H₂O photolysis. In this study, we use a plug-flow kinetic model to investigate OFR properties under a very wide range of conditions applicable to both field and laboratory studies. We show that the radical chemistry in OFRs can be characterized as a function of UV light intensity, H₂O concentration, and total external OH reactivity (OHR_{ext}, e.g., from volatile organic compounds (VOCs), NO_x, and SO₂). OH exposure is decreased by added external OH reactivity. OFR185 is especially sensitive to this effect at low UV intensity due to low primary OH production. OFR254 can be more resilient against OH suppression at high injected O₃ (e.g., 70 ppm), as a larger primary OH source from O₃, as well as enhanced recycling of HO₂ to OH, make external perturbations to the radical chemistry less significant. However if the external OH reactivity in OFR254 is much larger than OH reactivity from injected O₃, OH suppression can reach 2 orders of magnitude. For a typical input of 7 ppm O₃ (OHR_{O₃} = 10 s⁻¹), 10-fold OH suppression is observed at OHR_{ext} ~ 100 s⁻¹, which is similar or lower than used in many laboratory studies. The range of modeled OH suppression for literature experiments

is consistent with the measured values except for those with isoprene. The finding on OH suppression may have important implications for the interpretation of past laboratory studies, as applying OH_{exp} measurements acquired under different conditions could lead to over a 1-order-of-magnitude error in the estimated OH_{exp}. The uncertainties of key model outputs due to uncertainty in all rate constants and absorption cross-sections in the model are within ±25 % for OH exposure and within ±60 % for other parameters. These uncertainties are small relative to the dynamic range of outputs. Uncertainty analysis shows that most of the uncertainty is contributed by photolysis rates of O₃, O₂, and H₂O and reactions of OH and HO₂ with themselves or with some abundant species, i.e., O₃ and H₂O₂. OH_{exp} calculated from direct integration and estimated from SO₂ decay in the model with laminar and measured residence time distributions (RTDs) are generally within a factor of 2 from the plug-flow OH_{exp}. However, in the models with RTDs, OH_{exp} estimated from SO₂ is systematically lower than directly integrated OH_{exp} in the case of significant SO₂ consumption. We thus recommended using OH_{exp} estimated from the decay of the species under study when possible, to obtain the most appropriate information on photochemical aging in the OFR. Using HO_x-recycling vs. destructive external OH reactivity only leads to small changes in OH_{exp} under most conditions. Changing the identity (rate constant) of external OH reactants can result in substantial changes in OH_{exp} due to different reductions in

OH suppression as the reactant is consumed. We also report two equations for estimating OH exposure in OFR254. We find that the equation estimating OH_{exp} from measured O₃ consumption performs better than an alternative equation that does not use it, and thus recommend measuring both input and output O₃ concentrations in OFR254 experiments. This study contributes to establishing a firm and systematic understanding of the gas-phase HO_x and O_x chemistry in these reactors, and enables better experiment planning and interpretation as well as improved design of future reactors.

1 Introduction

Species emitted into the Earth's atmosphere are degraded by oxidative chemistry dominated by the OH radical. OH oxidation plays an important role in self-cleaning of the atmosphere (Levy II, 1971), O₃ production, and formation of secondary aerosols (Volkamer et al., 2006; Hallquist et al., 2009).

Because of the very low ambient concentrations of the atmospheric oxidants, oxidation timescales in the atmosphere can be long. They range from several hours (e.g., isoprene) to months (e.g., acetone) or longer (e.g., CH₄), which presents challenges for studying this chemistry directly in the atmosphere as other processes such as advection, deposition, mixing etc. happen in parallel. Atmospheric simulation chambers using UV light sources above 300 nm (e.g., UV blacklights or Xe arc lamps, or outdoor solar radiation) have been used for many decades to study atmospheric oxidation processes in a manner that decouples them from transport and other processes (Cocker et al., 2001; Carter et al., 2005; Presto et al., 2005; Wang et al., 2011; Platt et al., 2013). However such chambers have some shortcomings such as long simulation times of hours, inability to reach high OH exposures as needed to fully simulate long atmospheric residence times, significant wall loss of gases and particles, and difficulty in performing experiments with ambient air (George et al., 2007; Kang et al., 2007; Carlton et al., 2009; Seakins, 2010; Wang et al., 2011). An alternative type of reactor has been developed to overcome those limitations using lamps producing wavelengths not present in the troposphere to produce high oxidant concentrations, while allowing ambient air to flow through the reactor. For example, oxidation flow reactors (OFRs) using low-pressure Hg lamps can produce OH in large concentrations from H₂O and/or O₃ photolysis, enabling short residence times and hence reduce wall losses. In addition to use in reactors for atmospheric studies, chemistry initiated with low-pressure Hg lamps is also widely used in other fields, e.g., water and air purification (Legrini et al., 1993; Andreozzi et al., 1999; Johnson et al., 2014; Ye et al., 2014), chemical analysis (Danet et al., 2009; Ma and Xia, 2014), photochemical vapor deposition (Kumata et al.,

1986), and optical pumping for laser generation (Witte et al., 1979).

The UV light used in OFRs is typically either at 254 nm ("OFR254") or both 185 and 254 nm ("OFR185"). OFR254 requires the addition of externally formed O₃ since OH is formed only via O₃ photolysis at 254 nm. OFR185 does not require this addition since OH can be formed from H₂O photolysis at 185 nm. O₃ is also formed in OFR185 from O₂ photolysis at 185 nm. Because of their short experimental time scales and ease of use in the field, OFRs have gained popularity in both field and laboratory studies, in particular for research on secondary organic aerosols (SOA) (Massoli et al., 2010; Cubison et al., 2011; Kang et al., 2011; Lambe et al., 2011a, b, 2012, 2013; Bahreini et al., 2012; Saukko et al., 2012; Wang et al., 2012; Li et al., 2013; Ortega et al., 2013; Tkacik et al., 2014). These studies were conducted under a wide range of experimental conditions, e.g., relative humidity, UV light intensity, and VOC (volatile organic compounds) and NO_x concentrations.

In spite of the wide application of the radical chemistry in OFRs, the quantitative characterization of the radical chemistry itself has been extremely limited. To study the radical chemistry in OFRs experimentally, measurements of radicals over a very wide range of conditions would be needed, which are difficult and expensive to conduct. Modeling studies thus offer a very useful strategy for the characterization of OFR gas-phase radical chemistry. Although individual radical reactions relevant to OFRs with low-pressure Hg lamps are well known (Sander et al., 2011), to our knowledge, only two such modeling studies have been performed to date for OFR185 (Ono et al., 2014; Li et al., 2015), and none for OFR254. Ono et al. (2014) investigated the dependence of the consumption of O₃ and some radicals on H₂O concentration (abbr. H₂O hereinafter) in OFR185 with their model. The kinetic model that Li et al. (2015) developed compared well against measurements of OH exposure (OH_{exp}) and O₃ concentration (abbr. O₃ hereinafter) in laboratory calibration experiments and field studies using OFR185. They showed that OH exposure (OH_{exp}) in OFR185 increases strongly with UV light intensity (abbr. UV hereinafter), H₂O, and residence time, and decreases strongly with external OH reactivity ($\text{OHR}_{\text{ext}} = \sum_i k_i [R_i]$, where k_i and $[R_i]$ are the rate constant with OH and the concentration of the i th OH-consuming reactant in the system. This calculation excludes "internal" OH reactants, namely OH, HO₂, O₃, and H₂O₂). However these authors did not report any results for OFR254, nor did they quantify the parametric uncertainties in their models, consider cases with very high OHR_{ext} that have been used in multiple published experiments, or consider different types of OHR_{ext}.

In this paper, we use an improved version of the Li et al. (2015) model to systematically characterize the radical chemistry in OFRs as a function of the three main parameters: UV, H₂O, and OHR_{ext}. These are the parameters upon

which OH exposure in OFR185 has been shown to mainly depend (Li et al., 2015), and thus, we investigate a very large space spanned by these parameters, rather than choosing a few discrete points. We also study the effects of some additional parameters regulating the radical chemistry, i.e., extent of HO_x destruction vs. recycling by OHR_{ext}, the identity of the external OH reactants, and the amount of initially injected O₃ in OFR254. In addition, the uncertainties of kinetic parameters are considered in this study and the corresponding output uncertainties, as well as the contribution of key parameters to those uncertainties, are estimated by Monte Carlo uncertainty propagation. This study provides credible answers to key uncertainties about the chemistry in OFRs, thus enabling better experimental interpretation and design for future studies.

2 Methods

In this section, we briefly introduce the OFR we use (Sect. 2.1), and then describe the model and the experimental conditions for OFRs in this study (Sect. 2.2). The method for uncertainty and sensitivity analysis is presented in Sect. 2.3.

2.1 Potential Aerosol Mass flow reactor

Kang et al. (2007) introduced the Potential Aerosol Mass (PAM) flow reactor, an OFR designed for secondary aerosol formation studies. This type of OFR has been used by multiple groups, in particular to study SOA formation and aging (Massoli et al., 2010; Cubison et al., 2011; Kang et al., 2011; Lambe et al., 2011a, b, 2012, 2013; Bahreini et al., 2012; Saukko et al., 2012; Wang et al., 2012; Li et al., 2013; Ortega et al., 2013). Although earlier versions had different geometry, the version of the PAM reactor used in almost all publications and currently in use by all groups is a cylindrical vessel with an approximate volume of 13 L. Some versions are made completely of coated aluminum, while others are part aluminum and part glass. Low-pressure Hg UV lamps (model no. 82-9304-03, BHK Inc.) are installed inside the reactor to produce UV light at 185 and 254 nm. Experiments using 1, 2, and 4 lamps have been reported. The UV intensity can be rapidly changed via the Hg lamp voltages. The OFR185 mode uses Teflon sleeves for the lights, which transmits both wavelengths (Li et al., 2015), which allows ambient or sample air alone to be processed by the reactor. If quartz sleeves are used, the 185 nm light is removed, leaving photons at 254 nm for the photochemical generation of OH radicals (OFR254 mode). In that case, externally generated O₃ is introduced into the reactor, along with the ambient/sample air. As discussed below, the chemistry in OFR254 mode is strongly dependent on the amount of injected O₃. For this reason we will adopt the nomenclature OFR254-X where X is the injected O₃ concentration in ppm, e.g., OFR254-70 and OFR254-7 starting with 70 and 7 ppm O₃, respectively.

2.2 Model description

The model used in the present study is based on that of Li et al. (2015). It is a standard chemical-kinetic plug-flow model. Li et al.'s model includes all O_x and HO_x photolysis and thermal reactions whose kinetic data are available in the JPL chemical kinetic data evaluation (Sander et al., 2011) and several reactions involving external OH reactivity (e.g., from SO₂, CO and NO_x, see Table 1 of Li et al. (2015)). We implement this reaction scheme in the KinSim chemical kinetic integrator (<http://www.igorexchange.com/node/1333>) implemented in Igor Pro 6 (Wavemetrics, Lake Oswego, OR, USA). The stiff coupled system of ordinary differential equations is solved by the method of backward differentiation formula without any steady-state approximations using double precision variables. The integrator adaptively computes integration time steps that satisfy the mean square root of absolute error being lower than a threshold. To minimize the calculation time without diminishing the quality of the output concentrations, we set this threshold to 800 molecules cm⁻³, which is orders of magnitude smaller than the concentrations of all species in this model, except O(¹D). Furthermore, the O(¹D) concentration should be highly accurate, since it is controlled by extremely fast reactions with the most abundant species (e.g., O₂, N₂, and O₃) with negligible relative error (the absolute error threshold of 800 molecules cm⁻³ for those species' concentrations (> 10¹⁵ molecules cm⁻³) results in negligible relative error, so that relative errors propagated into O(¹D) concentration are also negligible). Compared to Li et al.'s model, this implementation in the KinSim integrator reduces the calculation time by a factor greater than 1000, allowing the exploration of the chemistry in a very large parameter (physical input conditions or kinetic parameters) space. The results of our independent implementation were found to be in agreement with those from the model of Li et al. (2015) within better than 1 % for all chemical species over a wide range of physical conditions.

In this study, we assume plug flow with a residence time of 180 s. Temperature and atmospheric pressure are set to 295 K and 835 mbar, respectively, which are typical values in Boulder, CO, USA. The range of H₂O mixing ratios studied is 0.07–2.3 % (equivalent to a relative humidity range of 3–90 % at 295 K). We study four levels of external OH reactivity (OHR_{ext}) representing the range in most field and laboratory studies: 0, 10, 100, and 1000 s⁻¹ (10 s⁻¹ is equivalent to ~ 4 ppb isoprene, ~ 8 ppb α-pinene, ~ 70 ppb toluene, or ~ 30 ppb *n*-dodecane, Fig. S1 in the Supplement). SO₂ is used as the surrogate of external OH reactivity. In a recent study, Bonn et al. (2014) measured OHR vs. time in a few VOC reactions and in some it decreased with time and in others it increased and later decreased because of the continuing reactivity of the products. Although SO₂ is consumed by OH much more slowly than most primary VOCs, it is actually more realistic in terms of the decrease of total OH reactivity than using only the first generation reaction of a

VOC. If we only consider the primary oxidation of VOCs, OHR_{ext}, due to most VOCs should very quickly decrease to ~ 0 , then has no effect during most of the residence time, leading to low effective OHR_{ext}. Actually, products of primary VOC oxidation can undergo further oxidation acting as external OH reactants. As a result, the decay of OHR_{ext} due to total VOCs is usually much slower than that due to primary VOCs. We thus believe that SO₂ can better capture the features of real OHR_{ext} decay and effective OHR_{ext}. Also, importantly, SO₂ + OH results in the production of HO₂ and thus is HO_x neutral. This is also applicable to reactions of OH with CO and (to a good approximation) VOCs, while OH + NO₂ does lead to HO_x destruction. The impact of HO_x conserving vs. destroying reaction and of the reaction rate of the OH reactant is investigated below. NO is quickly converted to NO₂ by the high levels of O₃ present, and NO₂ quickly forms HNO₃ by reaction with OH (Li et al., 2015). In the base case, SO₂ concentration decreases as it is consumed by OH in this study. In some additional cases, we also keep a constant OHR_{ext} or model different OHR_{ext} variations as surrogates of VOC oxidation (Fig. S2). For OFR254, we add 70 ppm externally formed O₃ (OFR254-70), as used in OFR254 experiments during the BEACHON-RoMBAS campaign (Palm et al., 2015), and also explore the chemistry when 7 ppm O₃ is added instead (OFR254-7), as has been done in other studies (Kang et al., 2011; Liu et al., 2015). The range of photon fluxes studied at 185 and 254 nm are 10¹¹–10¹⁴ and 4.2 × 10¹³–8.5 × 10¹⁵ photons cm⁻² s⁻¹, respectively, based on the characterization of Li et al. (2015). Within the ranges of the parameters explored, we also define several typical cases, which are labeled by two characters for low (L), medium (M), or high (H) H₂O and UV, respectively, and one character for 0, low (L), high (H), or very high (V) OHR_{ext} (Table 1).

2.3 Sensitivity and uncertainty analyses

It is of interest to characterize the degree of uncertainty of the outputs due to uncertain kinetic parameters, as well as the contributions of different parameters to the uncertainties of key outputs. For this analysis it is necessary to appropriately represent uncertain input kinetic parameters and propagate their uncertainties through the model. Note that because of the model's limitations, we do not assess the impact of some factors or input parameters that may lead to uncertain outputs, e.g., Hg lamp emission variations in space and time, variable UV fluxes at different points in the reactor, the assumption of plug flow, and the fact that temperature may vary by a few degrees due to incomplete removal of the lamp heat by the N₂ sheath flow. The effect of those parameters should be the focus of future studies.

2.3.1 Representation of uncertain kinetic parameters

To take parametric uncertainties into account, we use the formalism of the JPL chemical kinetic data evaluation (Sander et al., 2011). All uncertain rate constants and photoabsorption cross-sections (or partial cross-sections for multichannel photolysis) are assumed to have log-normal distributions, which ensure the positivity of these parameters and are commonly used to represent uncertainties in kinetic models (Hanna et al., 2001). The uncertainty factor f can be used as a measure of uncertainties of log-normally distributed random variables. It is defined as

$$f = e^{\sigma}, \quad (1)$$

where σ is the standard deviation of the random variable's logarithm. Numerically, a random variable's uncertainty factor is approximately equal to 1 plus its relative uncertainty if the uncertainty is relatively small. In the JPL database, uncertainty factors of rate constants are given only at 298 K. To estimate the corresponding uncertainty factors at 295 K, we apply the following formula recommended in the JPL data evaluation:

$$f(T) = f(298 \text{ K}) \exp \left[g \left(\frac{1}{T} - \frac{1}{298 \text{ K}} \right) \right], \quad (2)$$

where T is temperature (in K), and g is a constant that parameterizes the additional uncertainty arising from the temperature effect (in K). Uncertainty factors of a few (partial) absorption cross sections used in the present model are not available in the JPL database. We thus use the uncertainties recommended for these cross sections by Hébrard et al. (2006).

2.3.2 Monte Carlo uncertainty propagation

To propagate the parametric uncertainty into the model outputs, BIPM et al. (2008) recommend sample-based Monte Carlo uncertainty propagation (MCUP) methods. By MCUP, we propagate representative samples of the input distributions to obtain output distributions, from which we compute all necessary statistics. To perform MCUP in the present model, an appropriate sampling of all rate constants and cross-sections is necessary. Considering their log-normality, we generate the random samples by the following method (Peng et al., 2012):

$$\ln k_{ij} = \ln k_i^0 + \epsilon_j \ln f_i, \quad (3a)$$

$$\ln \sigma_{mn} = \ln \sigma_m^0 + \epsilon_n \ln f_m, \quad (3b)$$

where k_i^0 , f_i , and k_{ij} are the nominal value, the uncertainty factor, and the j th sample of the i th rate constant, respectively. ϵ_j is the j th sample of a random variable following the standard normal distribution. The (partial) cross-section samples, σ_{mn} , can be generated in the same way.

Table 1. Code of the labels of typical cases. A case label is composed of three characters denoting the water mixing ratio, the photon flux, and the external OH reactivity, respectively.

	Water mixing ratio	Photon flux	External OH reactivity
Options	L = low (0.07 %)	L = low (10^{11} photons $\text{cm}^{-2} \text{s}^{-1}$ at 185 nm; 4.2×10^{13} photons $\text{cm}^{-2} \text{s}^{-1}$ at 254 nm)	0
	M = medium (1 %)	M = medium (10^{13} photons $\text{cm}^{-2} \text{s}^{-1}$ at 185 nm; 1.4×10^{15} photons $\text{cm}^{-2} \text{s}^{-1}$ at 254 nm)	L = low (10 s^{-1})
	H = high (2.3 %)	H = high (10^{14} photons $\text{cm}^{-2} \text{s}^{-1}$ at 185 nm; 8.5×10^{15} photons $\text{cm}^{-2} \text{s}^{-1}$ at 254 nm)	H = high (100 s^{-1})
	* = the whole range	* = the whole range	V = very high (1000 s^{-1})
Examples	LH0:	low water mixing ratio, high photon flux, no external OH reactivity	
	M*H:	medium water mixing ratio, whole explored range of photon flux, high external OH reactivity	

2.3.3 Correlation-based parametric uncertainty analysis

Li et al. (2015) performed a study of the sensitivity of four key model outputs, i.e., OH_{exp} , average O_3 and H_2O_2 concentrations, and HO_2 / OH ratio, to model inputs of UV flux, pressure, temperature, residence time, H_2O , and OHR_{ext} . In the present work, we perform a complementary parametric uncertainty study that investigates the dependences of the same outputs, but on rate constants and absorption cross-sections. With the output from the Monte Carlo procedure from the previous section, we are able to calculate, at low computational expense, the relative contributions of the uncertain input parameters to the total output uncertainties.

The calculation of these relative contributions is a standard goal of uncertainty analysis (Saltelli et al., 2005). These contributions result from the amplification or reduction of the parameter uncertainties via the model during the propagation. Therefore, the contribution of a certain input parameter to the uncertainty of a given output depends on both the uncertainty on the parameter and the sensitivity of specific output to that input parameter (Saltelli et al., 2005; Wakelam et al., 2010).

To perform such an uncertainty analysis, we use a correlation-based method: we calculate the Spearman correlation coefficients between all model parameters and each of the four above-mentioned outputs, which is recommended for complex models (Wakelam et al., 2010). If higher-order effects are negligible, then the squared correlation coefficient between a model parameter and an output is equal to the corresponding parameter's relative contribution to the output (relative) variance (Saltelli et al., 2005). This method has been successfully applied to identify the reactions that have the most overall influence on the outputs in complex reaction networks (Peng et al., 2010, 2014; Gans et al., 2013). As

discussed below, we verify that the higher-order effects only account for a negligible or minor part of the output uncertainties in our model (see Sect. 3.3). We also ensure that the sample number (5000) is sufficiently large for a satisfactory convergence of the uncertainty analysis.

3 Results and discussions

In this section, we characterize the O_x and HO_x radical chemistry in both OFR185 and OFR254-70 as a function of the three most important inputs: H_2O , UV, and OHR_{ext} . We also show sensitivity analysis-related results, i.e., the output uncertainties and their apportionment to the input parameters

The cases with very high external OH reactivity (1000 s^{-1}) are not representative of ambient conditions, but rather are included to represent some laboratory experiments under very high reactant concentrations (Lambe et al., 2011b, 2015; Tkacik et al., 2014; Liu et al., 2015). Only key results for these cases are discussed in detail in this section, with most results being reported in the Supplement.

3.1 Main species and conversions

OFRs have high OH concentrations and active HO_x chemistry, as shown in Fig. 1 for the case with medium H_2O and UV, and zero OHR_{ext} (case MM0, cf. Table 1). For this case, OH concentrations in both OFR185 and OFR254-70 are of the order of magnitude of 10^{10} molecules cm^{-3} and thus ~ 4 orders of magnitude higher than typical ambient values (Stone et al., 2012). The O_3 and HO_2 concentrations are higher than ambient as well by several orders of magnitude. These higher concentrations of highly oxidative species are the key to the OFRs' short oxidation timescales.

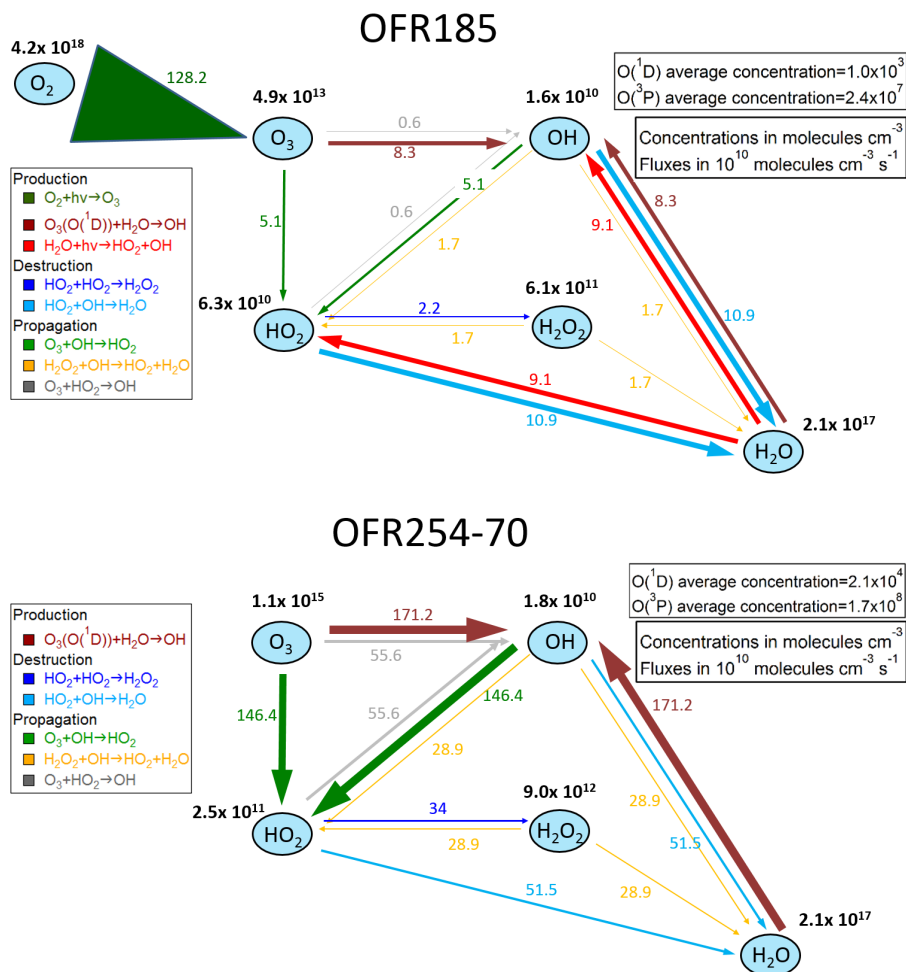
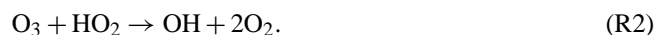


Figure 1. Schematics of main species and major reaction pathways for a case with medium H₂O and UV, and zero OHR_{ext}, for both OFR185 and OFR254-70. Species average concentrations (in molecules cm⁻³) are shown in black beside species names. Arrows denote directions of the conversions. Average reaction fluxes (in units of 10¹⁰ molecules cm⁻³ s⁻¹) are calculated according to the production rate, and shown on or beside the corresponding arrows and in the same color. Within each schematic, the thickness of the arrows is a measure of their corresponding species flux. Multiple arrows in the same color and pointing to the same species should be counted only once for reaction flux on a species. Note that all values in these schematics are average ones over the residence time, and not obtained from steady state. In the legend, reactions are classified as production, destruction, and propagation of HO_x. Since the reactions involving O and H atoms are very fast, they are not shown explicitly.

The arrows in Fig. 1 indicate how HO_x species are formed, interconverted, and consumed. Both reactors form primary OH from O₃ + 254 nm (via O₃ + 254 nm → O₂ + O(¹D) and O(¹D) + H₂O → 2OH), while OFR185 produces 70 % of its primary HO_x from H₂O + 185 nm. Note that the production, consumption, and interconversion of HO_x have average rates on the same order of magnitude *within* each type of OFR. This comparison reveals that the interconversion of HO_x is very active in these OFRs, even without an external OH reactant that converts OH into HO₂, e.g., SO₂. This interconversion is dominated by O₃ through the following reactions:



On the other hand, the interconversion of HO_x does not dominate over its primary production and final destruction. In both OFRs, the flux of OH → HO₂ is several times as large as that of HO₂ → OH. This implies that, on average, for each primary HO_x produced, it does not interconvert many times, but rather relatively quickly follows its destruction pathway to form H₂O or H₂O₂.

In OFR254-70, the production, consumption, and interconversion of HO_x are all 1–2 orders of magnitude faster than in OFR185. The faster conversions in OFR254-70 result from the substantial initial injection of O₃ in OFR254-

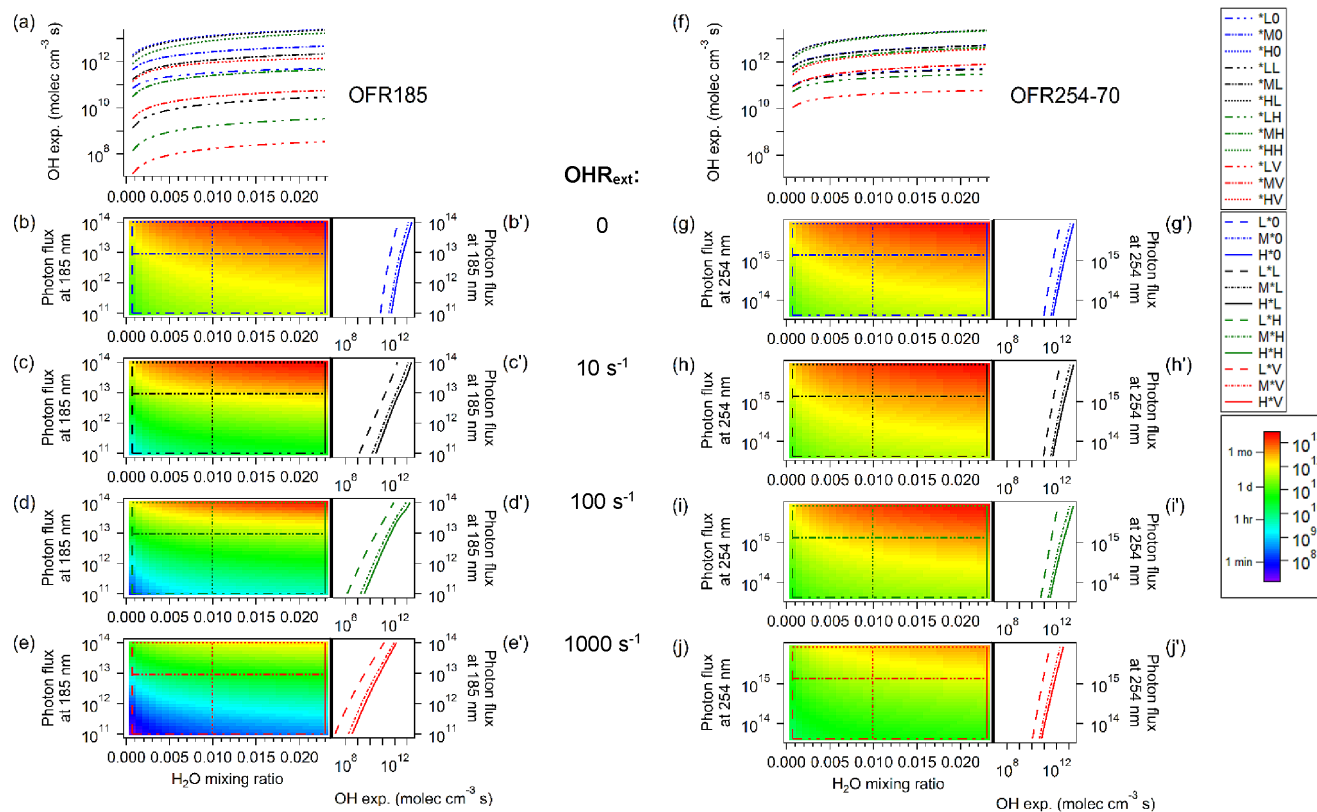


Figure 2. Dependence of OH exposures (in molecules $\text{cm}^{-3} \text{s}$) in OFR185 and OFR254-70 on H_2O and UV, for OHR_{ext} of (b, g) 0, (c, h) 10, (d, i) 100, and (e, j) 1000 s^{-1} . (a, f) and (b'–j') are the line plots of OH exposures of several typical cases. These cases are denoted in the image plots (b–j) by horizontal or vertical lines of the same color and pattern as in the line plots. In detail, the cut lines are in blue, black, dark green, and red in the plots for the cases of 0, low, high, and very high external OH reactivity, respectively. Horizontal sparse-dash-dot-dot, dash-dot-dot, and dotted lines mark low, medium, and high water mixing ratios, respectively (first legend box). Vertical dashed, dash-dot, and solid lines mark low, medium, and high photon fluxes, respectively (second legend box). Refer to Table 1 for more details on case labels. The color scale corresponds to all image plots. Equivalent ambient exposure time (based on average ambient OH concentration of 1.5×10^6 molecules cm^{-3} (Mao et al., 2009)) is also indicated in the color scale.

70, ~ 25 times more than the O_3 formed in OFR185 under these average conditions, as the latter is only formed internally from $\text{O}_2 + 185 \text{ nm}$.

3.2 Characterization of the radical chemistry vs. H_2O , UV, and OHR_{ext}

In this section, we explore the radical chemistry systematically as a function of input conditions through examination of the dependence of several output and internal chemistry parameters. We systematically compare the results for OFR254-70 and OFR185 for all parameters, and interpret the reasons for the observed trends.

3.2.1 OH and O_3 exposures

Figures 2 and 3 show OH and O_3 exposures, respectively, for both reactors as a function of H_2O , UV, and OHR_{ext} . The highest OH exposures are quite close in OFR185 and OFR254-70, as are the highest O_3 exposures. The high-

est OH and O_3 exposures are slightly larger than 10^{13} and 10^{17} molecules $\text{cm}^{-3} \text{s}$, respectively. OH_{exp} in both types of OFRs are similarly sensitive to the inputs (H_2O , UV, and OHR_{ext}) under the conditions of higher H_2O , UV, and lower OHR_{ext} . OFR185 is more sensitive to the inputs than OFR254-70 at lower H_2O and UV and high OHR_{ext} . OH and O_3 exposures in OFR185 can be 5 and 3 orders of magnitude lower than their highest values, respectively, over the range of conditions considered here. By contrast, in OFR254-70 the lowest OH_{exp} is only 2 orders of magnitude lower than its highest value, and O_3 exposure is almost independent of the explored conditions. The different dynamic ranges can be important when designing experiments across a wide range of OH_{exp} .

The difference between the O_3 exposures in OFR185 and OFR254-70 can be easily explained. O_3 in OFR254-70 depends on almost nothing but the initially injected amount, at least under the high injected amounts considered in our study (70 ppm). Only under the highest UV and H_2O condi-

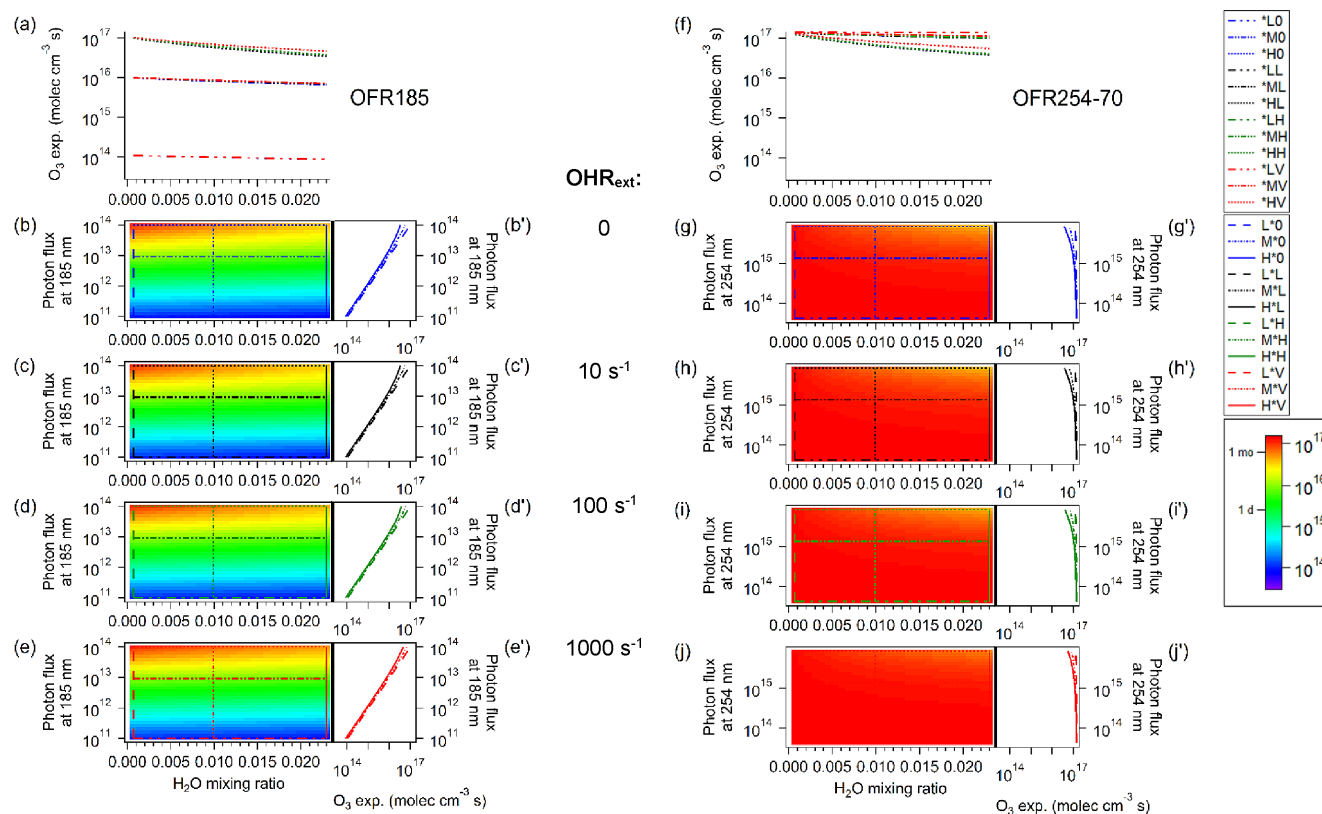


Figure 3. O₃ exposure (in molecules cm⁻³ s) vs. the same parameters and in the same format as Fig. 2. Equivalent ambient exposure time (based on average ambient O₃ mixing ratio of 34 ppb (Environment Canada, 2014)) is also indicated in the color scale.

tions does O₃ destruction by photolysis and HO_x recycling reactions result in a significant decrease in the O₃ concentrations. In OFR185, primary O₃ is exclusively produced via O₂ + 185 nm. Therefore, the O₃ production in OFR185 is nearly proportional to the photon flux at 185 nm (Fig. 3b'–d'). As the 185 nm flux spans 3 orders of magnitude, so does the O₃ exposure. The O₃ consumption in both OFRs is minor compared to the O₃ production under most conditions. Destruction of most O₃ by photons and HO_x only occurs under conditions where UV is high and H₂O is not too low (Fig. 3a, f, b'–j'). The very different exposures to O₃ in each OFR are important when considering species that react with both OH and O₃ such as monoterpenes.

In contrast, the reasons for the difference in OH_{exp} between OFR185 and OFR254-70 are complex. OH is formed through H₂O + 185 nm and O₃ + 254 nm in OFR185, and exclusively from the latter reaction in OFR254-70. Therefore, the primary production of OH in both cases should be approximately proportional to the water vapor concentration, photon flux, and O₃ concentration. In our base case O₃ is much higher in OFR254-70, resulting in a much stronger primary OH source that makes the chemistry more resilient to external perturbation. In addition, the consumption of OH due to OHR_{ext} in both cases should be trivially proportional

to OHR_{ext}. Thus, this different behavior of the OH exposures in the two OFRs should result from differences in the HO_x chemistry of the OFRs.

Indeed the interconversion of OH and HO₂, shown in the previous section to be greatly enhanced by the injected O₃ in OFR254-70, plays an important role on the observed differences. In cases with substantial external consumption of OH (Fig. 2c, d, h, i), the rapid interconversion of OH and HO₂ in OFR254-70 buffers the OH concentration by producing OH from the more abundant HO₂. The higher the O₃ concentration, the stronger the buffering effect. Consequently, OH_{exp} is much less sensitive to OHR_{ext} in OFR254-70 under these conditions (Fig. 2h, i), than in OFR185 (Fig. 2c, d). In other words, the recycling of OH from O₃ + HO₂ buffers the consumption of OH.

3.2.2 OH reactivity (OHR)

The O₃ buffering effect can be investigated more quantitatively by considering OHR, the inverse of the OH lifetime and a direct measure of OH consumption rate. OHR_{tot}, i.e., the sum of OHR_{ext} from external reactants such as SO₂ and OHR_{int} from internal reactants such as HO₂ and O₃ (including the injected O₃ in OFR254), is shown vs. operating con-

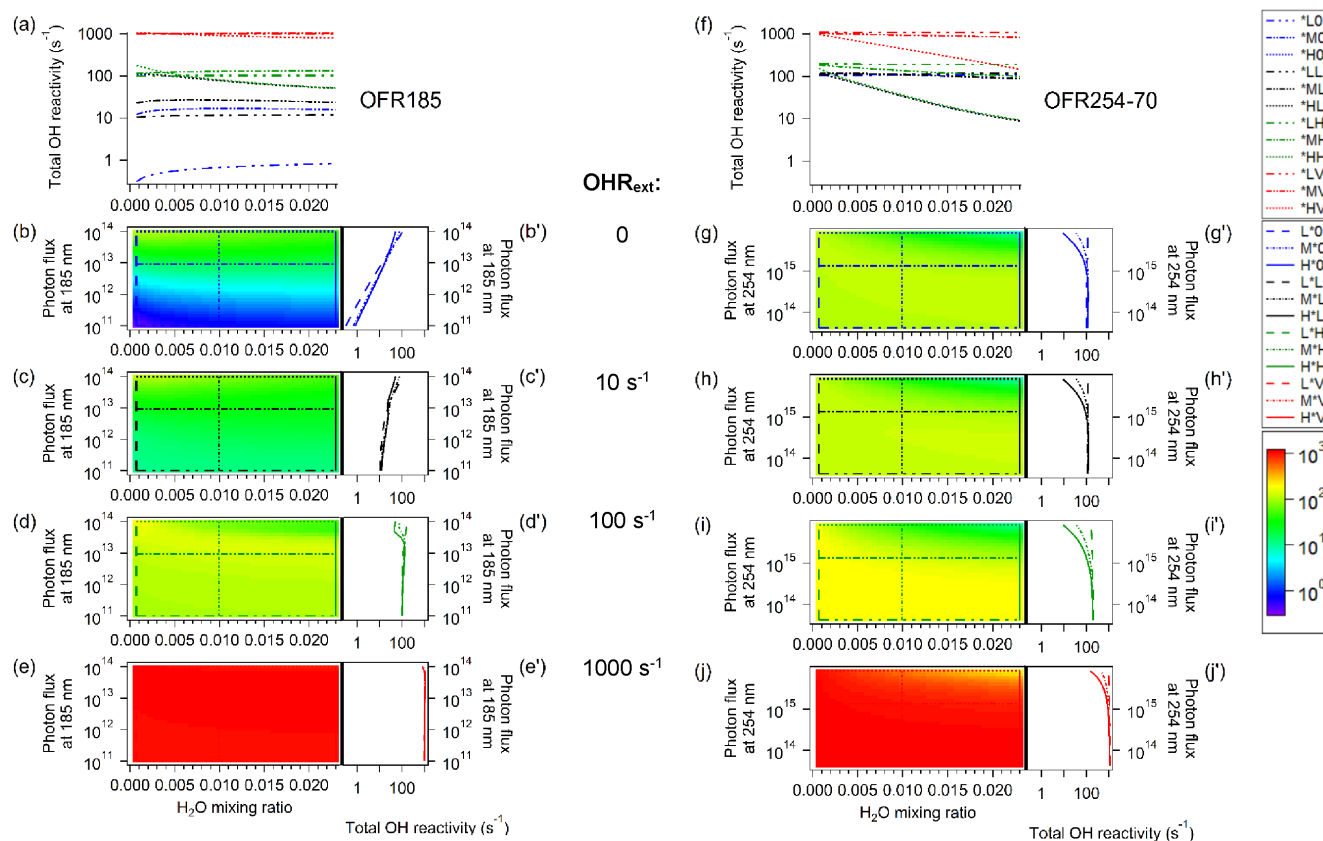


Figure 4. Total OH reactivity (in s^{-1}) vs. the same parameters and in the same format Fig. 2.

ditions in Fig. 4. The OHR_{tot} in Fig. 4b, g is just the *internal OH reactivity*, as there is no OHR_{ext} . As expected for this case, the major components of OHR_{int} are O_3 , H_2O_2 , HO_2 , and OH itself.

In OFR185, a strong UV dependence is observed in OHR_{int} Fig. 4b, b': from $\sim 1 \text{ s}^{-1}$ in the low-UV cases to $\sim 100 \text{ s}^{-1}$ in the high-UV cases. H_2O has only a minor influence on OHR_{int} . At low UV and H_2O , increasing H_2O leads to a HO_x source and thus increasing OHR_{int} . In the case of high UV, a high H_2O results in increasing concentrations of HO_x that cause a significant loss of O_3 and a net decrease in OHR_{int} .

As OHR_{ext} increases, the dependence of OHR_{tot} on UV in OFR185 is weakened (Fig. 4c, d, c', d'). We observe that OHR_{tot} is roughly equal to the sum of initial OHR_{ext} plus OHR_{int} from the case without OHR_{ext} . Although OHR_{ext} can be significantly reduced by the reaction with OH at medium and high UV, the resulting HO_2 and H_2O_2 produced from HO_2 increase OHR_{int} . Thus, the net change in OHR_{tot} is minor. However, the increase in OHR_{int} is slightly greater than the decrease in OHR_{ext} , in agreement with Li et al. (2015), as HO_2 and H_2O_2 are more reactive with OH than SO_2 . Therefore, at medium and high UV, the relative contribution of OHR_{int} to OHR_{tot} is significantly higher than the values es-

timated from initial OHR_{ext} and OHR_{int} in the case without OHR_{ext} (Fig. S3b, c, b', c'). However, at low UV, the amount of OH is not sufficient to cause a significant consumption of SO_2 , and OHR_{int} is much lower than OHR_{ext} . As a result, OHR_{ext} dominates OHR_{tot} at low UV, which explains the remarkably low OH_{exp} at low UV and high OHR_{ext} in OFR185.

In contrast to OFR185, in OFR254-70 (with 70 ppm O_3 input) OHR_{ext} never becomes dominant under the conditions of $\text{OHR}_{\text{ext}} = 0\text{--}100 \text{ s}^{-1}$ (Fig. S3e–g, f', g'). OHR_{int} accounts for $> 90\%$ and $> 50\%$ of OHR_{tot} for the cases with 10 and 100 s^{-1} OHR_{ext} , respectively. The amount of O_3 injected contributes $\text{OHR}_{\text{int}} = 101 \text{ s}^{-1}$, which is in agreement with an almost uniform OHR_{int} of $\sim 100 \text{ s}^{-1}$ in all cases except with high H_2O and UV, and the OHR_{tot} shown in Fig. 4f–i, g'–i'. At high H_2O and UV levels, in both OFR185 and OFR254-70, very large concentrations of OH radicals are formed and consume most external OH reactant, resulting in an OHR_{int} dominating OHR_{tot} (Fig. S3). Interestingly, under this condition, almost all O_3 ($> 90\%$) is also consumed in OFR254-70, leading to the only observed significant OHR_{tot} decrease for OFR254-70 (Fig. 4f–i, g'–i'), which, in part, contribute to the highest observed OH_{exp} reached by OFR254-70 (Fig. 2g–i, g'–i').

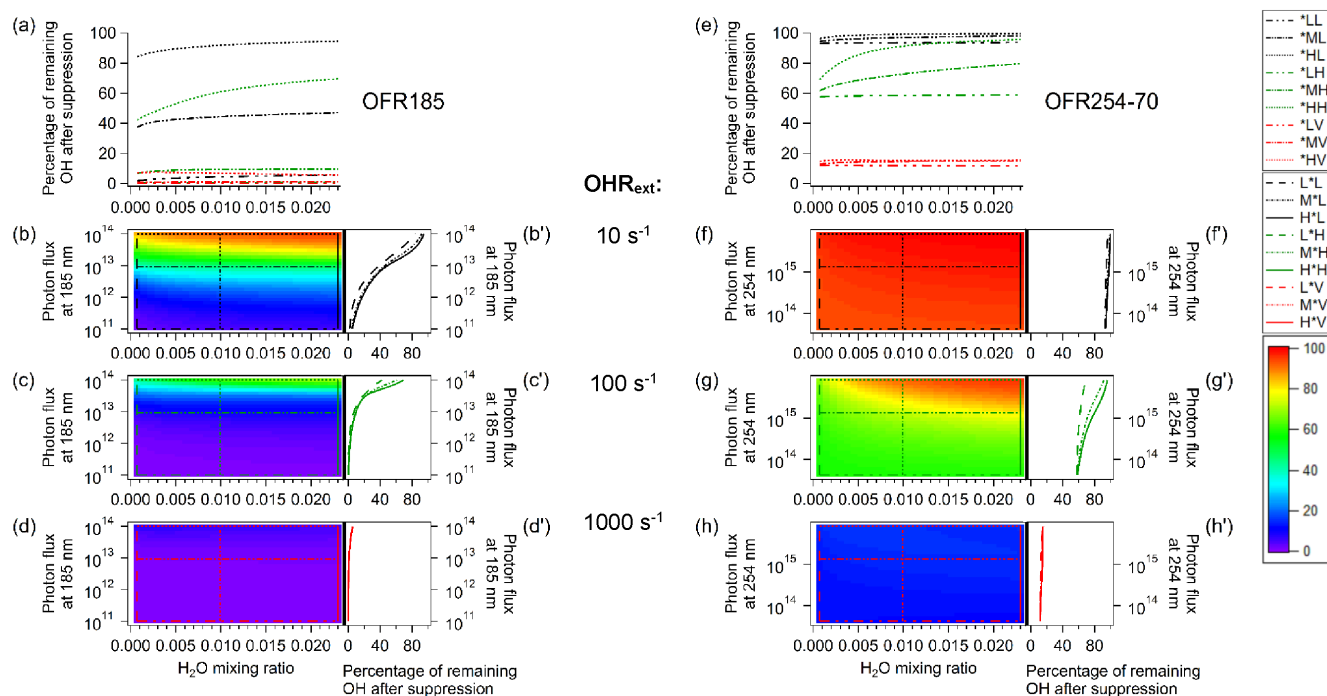


Figure 5. Percentage of remaining OH after suppression vs. the same parameters and in the same format Fig. 2, but without the case of no external OH reactivity, which is the reference case.

3.2.3 OH suppression

The changes in OH_{exp} can also be described in terms of OH suppression, i.e., the decrease of OH concentration caused by an addition of OHR_{ext} (Li et al., 2015). OH can be greatly suppressed in OFR185 if OHR_{ext} is high (Li et al., 2015), as shown in Figs. 5a–c, b', c' and S4. For OHR_{ext} = 100 s⁻¹, OH suppression is larger than 80 % except for high UV cases. This is due to rapid conversion for OH to HO₂ by OHR_{ext}, while HO₂ cannot be quickly recycled back to OH due to relatively low levels of O₃. In contrast, for OHR_{ext} ≤ 100 s⁻¹, OH in OFR254-70 is at most suppressed by ~ 50 % (Fig. S4), and less for the cases with a high H₂O or UV (Fig. 5f–i, h', i'). The injected O₃ in OFR254-70 explains the large difference between the reactors: it primarily produces much OH, recycles HO₂ to OH and thus prevents the latter from being largely suppressed. Interestingly the suppression of OH is not accompanied by a suppression of total HO_x, as illustrated in Fig. S5. Total HO_x remains approximately constant in OFR254-70 independently of OHR_{ext} in the cases with OHR_{ext} = 10 and 100 s⁻¹, as the fast recycling of OH and HO₂ by O₃ is predominant in the reactivity of both species. Total HO_x actually increases up to a factor of ~ 2 in OFR185, especially on the conditions that lead to OH suppression, as OH is converted to HO₂ and the total HO_x loss is reduced.

3.2.4 OFR conditions at very high OHR_{ext}

Very high OHR_{ext} of the order 1000 s⁻¹ or more has been used in some laboratory and field experiments (Lambe et al., 2011b; Tkacik et al., 2014; Liu et al., 2015), and thus it is of interest to explore the changes in OFR performance under these conditions. The chemistry in the cases with a very high OHR_{ext} (1000 s⁻¹) (Fig. 2–5, S3) retains all trends with the increasing OHR_{ext} discussed above. O₃ is still only slightly affected by OHR_{ext} (Fig. 3a, e, f, j, e', j'). In most cases, OHR_{tot} reaches the 1000 s⁻¹ level (Fig. 4a, e, f, j, e', j'), to which OHR_{ext} is the dominant contribution, since the OHR_{int} in both OFR185 and OFR254-70 only reaches ~ 100 s⁻¹. Under high H₂O and high UV conditions, strong OH production still leads to substantial consumption of the external OH reactant, which makes the reduced OHR_{ext} comparable to OHR_{int} (Fig. S3a, d, e, h, d', h'). These trends are also consistent with the changes of OH_{exp}, which is further lowered/suppressed at OHR_{ext} of 1000 s⁻¹ (Figs. 2a, e, f, j, e', j' and 5a, d, e, h, d', h'). O₃-promoted HO₂-to-OH recycling is always pronounced and systematically makes OH in OFR254-70 more resilient to the increase of OHR_{ext}, although OH suppression still reaches a factor of 8. Total HO_x at high H₂O and UV in OFR254-70 increases by a factor of ~ 2 (Fig. S5e, h, h'), as most O₃ is consumed and OH is converted to HO₂ by the external OH reactant. At these very high OHR_{ext}, OFR185 can only achieve substantial OH_{exp} at medium to high UV levels and is not useful at low UV

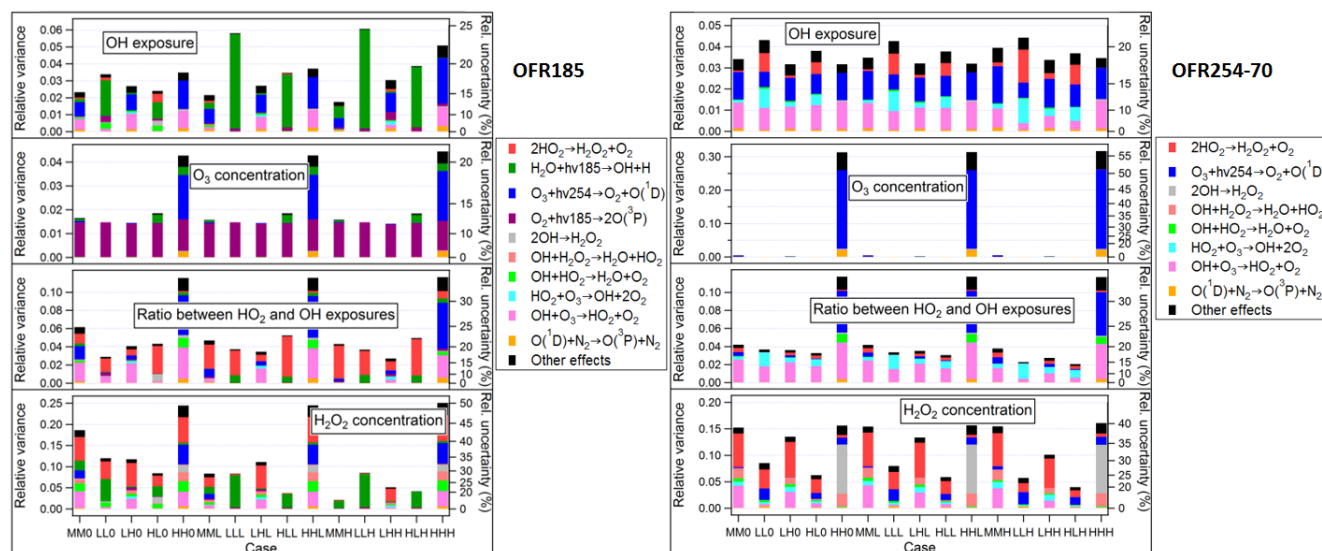


Figure 6. Relative variances (left axes)/uncertainties (right axes) of the outputs (i.e., OH exposure, O₃ concentration, ratios between HO₂ and OH exposure, and H₂O₂ concentration) of Monte Carlo uncertainty propagation, and relative contributions of key reactions to these relative variances in typical cases in OFR185 and OFR254-70. Relative variances are shown in linear scales (left axis), while corresponding relative uncertainties, equal to relative variances' square roots, are indicated by the non-linear right axis. Only the reactions with a contribution of no less than 0.04 to at least 1 relative variance are shown.

levels unless very low OH_{exp} are desired. Very high OHR_{ext} also results in much increased relative importance of non-OH driven reactions in both OFRs. Under those conditions, OH is heavily suppressed while other reactants that can consume some types of VOCs, e.g., 185 and 254 nm photons for aromatics and O₃ for alkenes, may not be significantly affected compared to moderate OHR_{ext} cases. Thus, those non-OH reactants may destroy comparable or larger amounts of VOCs than OH does at very high OHR_{ext}. This issue is investigated in detail in Peng et al. (2015).

3.3 Parametric uncertainty analysis

In this section, we quantify the uncertainties on the model outputs due to the uncertainty in model parameters (rate constants and (partial) cross-sections), and compare them with the dynamic ranges of some outputs to confirm the reliability of the results shown in the previous section. With the statistical samples of uncertain inputs and outputs, we can also perform an analysis to determine the reactions that contribute the most to output uncertainties.

3.3.1 Output uncertainty

We observe, over a wide range of conditions for both OFR185 and OFR254-70 (Fig. 6), moderate uncertainties (bar heights in Fig. 6) of the four key outputs: OH_{exp}, O₃, HO₂/OH, and H₂O₂. In most cases, the relative uncertainties of these outputs (1 standard deviation) are lower than 40%. None of the relative uncertainties that we obtained are higher than 56%. For the most important output, OH_{exp}, the

typical relative uncertainty is 15–20% for both OFR185 and OFR254-70, with a few cases reaching ~25%. This relative uncertainty is remarkably low and strongly suggests that the kinetic and photolysis parameters are not the dominant uncertainty sources in the system. Compared to the dynamic ranges of OH and O₃ exposures, which span ~5 and ~3 orders of magnitude in OFR185 and ~3 and 1/2 orders of magnitude in OFR254-70, these output relative uncertainties are generally quite low. In other words, the kinetic and photolysis parameters used in this study are known well enough to ensure reliable findings of the changes in chemistry with model inputs, within the physical assumptions of the model. The uncertainties in comparing the model results to experiments are likely dominated by the simplifications introduced in the model (e.g., uniform radiation field and no wall effects), as well as by incomplete information about the experimental inputs (e.g., dependence of UV light output on ambient temperature and lamp age, quantification of OHR_{ext} from primary VOCs and their oxidation intermediates, limited knowledge of species entering the reactor in field studies, etc.).

3.3.2 Reactions contributing the most to the parametric uncertainty

It is of interest to characterize which reactions substantially contribute to the output uncertainties. We consider reactions with correlation coefficients between its kinetic parameter and outputs larger than 0.2 as reactions that contribute significant uncertainty. This criterion has been previously applied

for similar analyses (Hébrard et al., 2009; Peng et al., 2010). A total of 10 reactions (out of 46 included in the model) are identified as controlling the parametric uncertainty of this model. These include the photolyses of the major species (H₂O and O₂ in OFR185; O₃ in both OFRs) and reactions of OH and HO₂ with themselves or some abundant species, i.e., O₃ and H₂O₂. We have discussed the importance of OH and HO₂ reactions in the gas-phase chemistry in OFRs previously. Initiation steps such as photolysis are highly influential in complex reaction networks (Peng et al., 2010). Thus, it is natural that these reactions appear as key contributors.

The photolyses of H₂O and O₂, which are the main pathways of primary OH and O₃ production in OFR185, respectively, are generally the most important contributors to the parametric uncertainty in OH_{exp} and O₃, respectively. O₃ + 254 nm also contributes to the uncertainty of both parameters in some cases. HO₂ / OH and H₂O₂, which involve non-primary products, are significantly influenced by more reactions in OFR185 compared to OH_{exp} and O₃, some of the most important being HO₂ + HO₂ and OH + O₃.

In OFR254-70, OH is not produced by photolysis of H₂O, but only O₃ + 254 nm. Therefore, photolysis of ozone is always an important contributor to the uncertainty on OH_{exp}. The reaction OH + O₃ is typically of comparable magnitude to O₃ photolysis, with the reactions HO₂ + O₃ and HO₂ self-reaction typically comprising the balance. Because of the large amount of O₃ injected and since input uncertainties are not considered in this analysis, O₃ (at the exit of the reactor) has very low parametric uncertainty, except for cases with high H₂O and UV where a larger fraction of the injected O₃ is consumed by photons. HO₂ / OH and H₂O₂ also have many uncertainty contributions, as in OFR185, with the most important for HO₂ / OH being OH + O₃, HO₂ + O₃ and sometimes (high UV and H₂O) O₃ photolysis and OH + HO₂. The largest contributors to the uncertainty of modeled H₂O₂ are the HO₂ and OH self-reactions, with smaller contributions from OH + O₃, OH + H₂O₂, and O₃ photolysis, but with quite variable proportions for the different cases. In OFR254-70, the recycling of HO₂ to OH is of remarkably higher importance than in OFR185, especially for OH_{exp} and HO₂ / OH, which are the outputs directly affected by these conversions.

3.4 Effects of several additional parameters

In addition to the major parameters altering the OFR radical chemistry (i.e., H₂O, UV, and OHR_{ext}), we investigate here the effects of some other parameters, i.e., difference between non-destructive and destructive OHR_{ext} (in terms of HO_x), the identity of external OH reactants, and the amount of injected O₃ in OFR254, by comparison with the base case, i.e., the case studied in Sect. 3.2.

3.4.1 Non-HO_x-destructive vs. HO_x-destructive OHR_{ext}

The consumption of OH by SO₂ leads to the production of HO₂, which does not lower the total amount of HO_x. Although this HO₂ regeneration also extensively exists in VOC oxidation, it is important to have a better understanding on the impact of destructive external OH reactants, i.e., external OH reactants whose OH-consuming process is not coupled with HO₂ regeneration, e.g., OH + NO₂ + M → HNO₃ + M, an important reaction in the OFR of Tkacik et al. (2014) because of the presence of large amount of NO_x in the source air in their study. To more clearly isolate the effect of HO_x-destructive vs. non-HO_x-destructive OHR_{ext}, we use SO₂ as the external OH reactant for both cases, but for the probing of the HO_x-destructive OHR_{ext} assume that the HO₂ regeneration reaction HSO₃ + O₂ → SO₃ + HO₂ does not occur.

The absence of HO₂ regeneration has mostly minor effects on OH_{exp}, as shown in Fig. 7, except for OFR254-70 at low UV and both OFRs at high H₂O and UV and very high OHR_{ext}. For OFR185 (Fig. 7a–d, b'–d'), under most conditions, OH_{exp} is very close to the value in the base case (Fig. 2). At the highest UV and OHR_{ext} ≤ 100 s⁻¹, photolysis dominates OH production, while the contribution of the recycling of HO₂ generated from SO₂ consumption to OH is small. At low UV, OH production from photolysis is weak, but the recycling of HO₂ generated from SO₂ consumption to OH becomes even weaker because of not only less OH that can be converted into HO₂ by SO₂, but also less O₃ that can recycle HO₂ to OH. Only under two particular conditions: (i) at high H₂O, high OHR_{ext} and UV at 185 nm around 3 × 10¹³ photons cm⁻² s⁻¹, and (ii) at high H₂O and UV and very high OHR_{ext}, a significant increase in OH_{exp} relative to the base case is observed (Fig. 7c, d, c', d'), because the reduced OH consumption by the lower HO₂ and H₂O₂ is important under these conditions.

For OFR254-70, under low-OHR_{ext} conditions, OH production by photolysis is high enough and/or HO₂ regeneration coupled with SO₂ consumption is low enough to prevent the regeneration of HO₂ from being a major effect (Fig. 7e–h, f'–h'). However, at low H₂O, low UV, and high/very high OHR_{ext}, the lack of HO₂ production from OHR_{ext} does cause a significantly lower OH_{exp} (Fig. 7e, g, h, g', h'), because under these conditions the reduction in OH recycling by HO₂ + O₃ is important. This effect can reach 1 order of magnitude at the lowest UV. In addition, at high H₂O and UV and very high OHR_{ext}, OH_{exp} increases significantly relative to the corresponding base case, for the same reason as in OFR185.

3.4.2 Identity of external OH reactants

The use of SO₂ as the surrogate of external OH reactants is a simplification in this study. In actual OFR experiments, external OH reactants can also be NO_x, CO, CH₄, and vari-

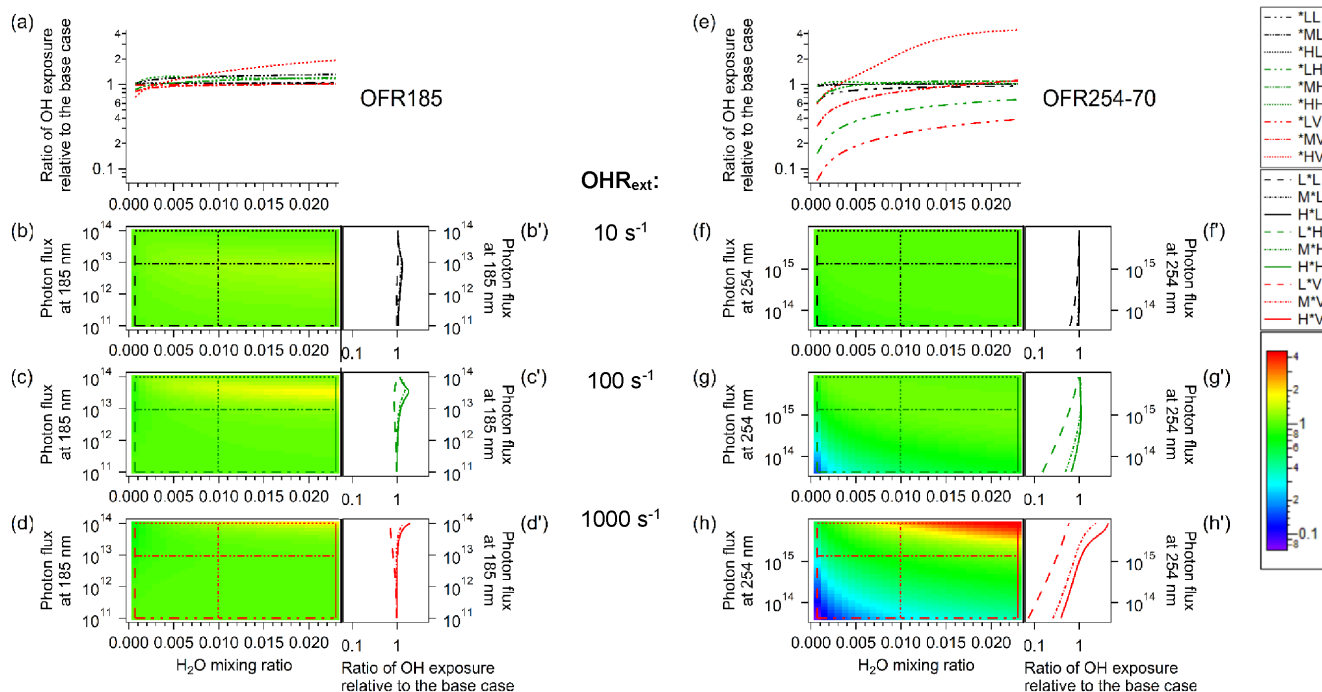


Figure 7. Percentage of OH exposure in the case of HO_x-destructive external OH reactivity (OHR_{ext}) relative to that in the base case (Fig. 2) vs. the same parameters and in the same format as Fig. 2, but for the cases of low (10 s^{-1}), high (100 s^{-1}), and very high (1000 s^{-1}) external OH reactivity.

ous VOC and their oxidation products. These reactants have a wide range of rate constants with OH, and the relative decrease of OHR_{ext} with time in the OFR can thus vary substantially between these cases. To bound the importance of this effect we study two extreme regimes, i.e., one where OHR_{ext} does not decay at all, and one where the external OH reactant is consumed at the collision rate. In both cases the products of the initial reaction are not explicitly represented in the model. For VOC reactions the former case is more realistic, as the constant OHR_{ext} can be thought to represent the reactivity of several generations of products as the initial reactant is consumed.

The effects of this parameter are shown in Figs. S6 and S7, and can be understood in terms of the impact of OHR_{ext} on reducing OH_{exp} illustrated in Figs. 2 and 5. When using a constant OHR_{ext} instead of SO_2 (Fig. S6), OH_{exp} is reduced similarly in both OFR for high UV and H_2O conditions. These were the conditions where a substantial fraction of the injected SO_2 was consumed in the reactor, thus keeping OHR_{ext} constant instead leads to up to factors of 2–3 reduction in OH_{exp} . The effect increases with OHR_{ext} as expected.

The effect of replacing SO_2 by a reactant with collision rate is more dramatic in OFR185 than for OFR254-70. OFR254 is more sensitive at lower input O_3 . Note that to achieve the same initial OHR_{ext} , the concentration of the reactant is ~ 300 times lower than for the SO_2 case. Therefore

the reactant is quickly consumed at short reaction times and for the rest of the residence time the OFRs revert to conditions with low OHR_{ext} (e.g., Fig. 2b, g). Thus, the integrated OH concentration, i.e., OH_{exp} is still suppressed relative to the no OHR_{ext} case but not as much as if all the OHR_{ext} is due to SO_2 . In particular, OH_{exp} increases strongly in the cases in which OH suppression was important and when the consumption of external OH reactant is significant, i.e., OFR185 at relatively low UV and/or H_2O but not at the lowest UV and H_2O . The effect reaches a factor of ~ 40 for OFR185 but only ~ 2 for OFR254-70, consistent with the much larger OH suppression in the former.

In summary, the identity of the OH reactant can make a substantial difference on OH_{exp} for OFR185 and very fast reacting species, and less so for other cases. However, note that this substantial difference is likely an artifact due to our simplified modeling for this case. In our model, there is no regeneration of external OH reactant (SO_2) after its consumption, while in reality, no VOC can be completely oxidized in only one step and most VOC oxidation intermediates also act as external OH reactants. Thus, it is very unlikely that OHR_{ext} in real cases can drop as quickly as shown in this case, even though the primary oxidation rate of some VOCs (e.g., isoprene) can be close to the collision rate.

3.4.3 Amount of injected O₃ in OFR254

The amount of injected O₃ is also a factor that may alter the chemistry in OFR254. In the BEACHON-RoMBAS campaign (Palm et al., 2015), 70 ppm O₃ was used in OFR254 to ensure that high OH exposures were reached, while O₃ was 9 and 27 ppm in Kang et al., and Lambe et al.'s laboratory studies, respectively (Kang et al., 2011; Lambe et al., 2011b). Thus, it is of interest to investigate the effect of a lower amount of injected O₃ on the OFR254 chemistry (compared to the base case of 70 ppm used in all other model runs in our study).

The ratio of OH_{exp} in OFR254-7 to that in OFR254-70 is shown in Fig. 8. At 0 OHR_{ext} (Fig. 8b, b'), OH_{exp} in OFR254-7 is ~40–80 % of that in OFR254-70, despite a lower initial O₃ concentration by a factor of 10. This relatively small difference in OH_{exp} is due to both OH production and consumption that are slowed down simultaneously: with less O₃, OH production through O₃ photolysis is weaker, although less than linearly as the UV light is less attenuated by the lower O₃. OH consumption by internal OH reactants, e.g., O₃, HO₂, and H₂O₂, is also weaker, because of less HO₂ formation through OH + O₃ → HO₂ + O₂, as well as lower H₂O₂ formation.

However, as OHR_{ext} increases, SO₂ contributes increasingly to OH consumption. The case with OHR_{ext} = 10 s⁻¹ gives similar results to the one without OHR_{ext}, as the OHR_{int} from O₃ is also 10 s⁻¹, and the reactor chemistry is not overwhelmed by OHR_{ext}. However when OHR_{ext} = 100 (Fig. 8d, d') and 1000 s⁻¹ (Fig. 8e, e'), the external reactivity does overwhelm the internal one, and strong OH suppression up to 2 orders of magnitude is observed, similar to what was discussed above for some conditions in OFR185. OH primary production from O₃ + 254 nm and its recycling from O₃ + HO₂ are smaller compared to the consumption by SO₂.

3.5 Effect of non-plug flow

In most of this paper we use the plug-flow assumption to allow interpreting any trends as being due to chemistry only. However, it is of interest to evaluate the impact of a non-plug-flow RTD (residence time distribution) over a wider range of conditions. Li et al. (2015) reported, for a typical OFR185 case, a 10 % change in average OH_{exp} when using the RTD reported by Lambe et al. (2011a). An OFR with a complex RTD can be approximately simulated as a set of plug-flow OFRs with different residence times. We thus calculate the outputs (i.e., OH_{exp}, O₃, SO₂ etc.) as a function of residence time using our plug-flow model, then compute their average values as the weighted average according to a specified RTD. A more complete simulation would involve the use of computational fluid dynamics software, along with diffusion and the three-dimensional UV light fields, which is outside the scope of the present paper.

We perform the calculations for OFR185, OFR254-70, and OFR254-7. In each case we simulate two RTDs, one for fully developed laminar flow in a cylindrical tube (Mory, 2013), and the measured PAM RTD reported in Lambe et al. (2011a), shown in Figure S8. The use of both non-plug-flow RTDs allows a first evaluation of the importance of the shape of the RTD on the results. This is useful because some OFRs such as Toronto Photooxidation Tube (TPOT) (George et al., 2007) are closer to a cylindrical tube, and also because some field applications of the PAM OFR do not use an inlet plate (Ortega et al., 2013, 2015) and are expected to have a less-skewed RTD than reported by Lambe et al. (2011a).

Figure 9 compares OH_{exp} for both RTDs and the plug-flow case. The difference is quantified as the average ratio of OH_{exp} calculated from direct mathematical integration for each RTD case (OH_{exp,RTD}^{MATH}) to OH_{exp} in the plug-flow case (OH_{exp,PF}). The average ratios are, for OFR185, 0.83 and 1.75 for the laminar and Lambe RTDs, respectively, and, for OFR254 (including both OFR254-70 and OFR254-7), 0.86 and 1.42, respectively. The differences for the laminar RTD are smaller than the parametric uncertainty of the model due to uncertain chemistry parameters (Sect. 3.3). Considering all cases of OFR185 and OFR254 combined, all cases with the laminar RTD are within a factor of 2 from the plug-flow OH_{exp}, while a few percent of the Lambe RTD cases (under extreme conditions) are outside the range of a factor of 2 from OH_{exp,PF}. Within the datapoints for the Lambe RTD, those at lower OHR_{ext} are close to the corresponding plug-flow points, in agreement with Li et al. (2015). At very high OHR_{ext} (1000 s⁻¹), and in particular, at high H₂O and UV in OFR185, the deviations between the Lambe-RTD and plug-flow OH_{exp} can be larger (Fig. S9).

In the cases of low OHR_{ext}, the generally small differences can be explained by the fact that OH reaches steady state very quickly (Li et al., 2015). Once this steady state is reached, OH does not vary substantially with reaction time under most conditions (Fig. S10), since the OH production and consumption rates are roughly balanced. If OH remains roughly constant during the residence time, OH_{exp} varies linearly with residence time. Thus, under these conditions, OH_{exp,PF} should be close to the average OH_{exp,RTD} for any RTD. However, at high UV and very high OHR_{ext}, the following two conditions are simultaneously met: (i) OHR_{ext} plays a dominant role in suppressing OH; (ii) the consumption of the external OH reactant is substantial (Fig. S10). In this case, OH significantly increases as the external OH reactant is consumed. This causes OH_{exp,RTD}^{MATH} to depend nonlinearly on residence time. The Lambe RTD has a large portion at residence times much longer than the average value (> 350 s), when almost all external OH reactant is destroyed and OH is approximately 1 order of magnitude higher than at the average residence time (180 s). This results in higher average OH_{exp,RTD}^{MATH} with the measured RTD than OH_{exp,PF} in OFR185. By contrast, the laminar RTD only has a very mi-

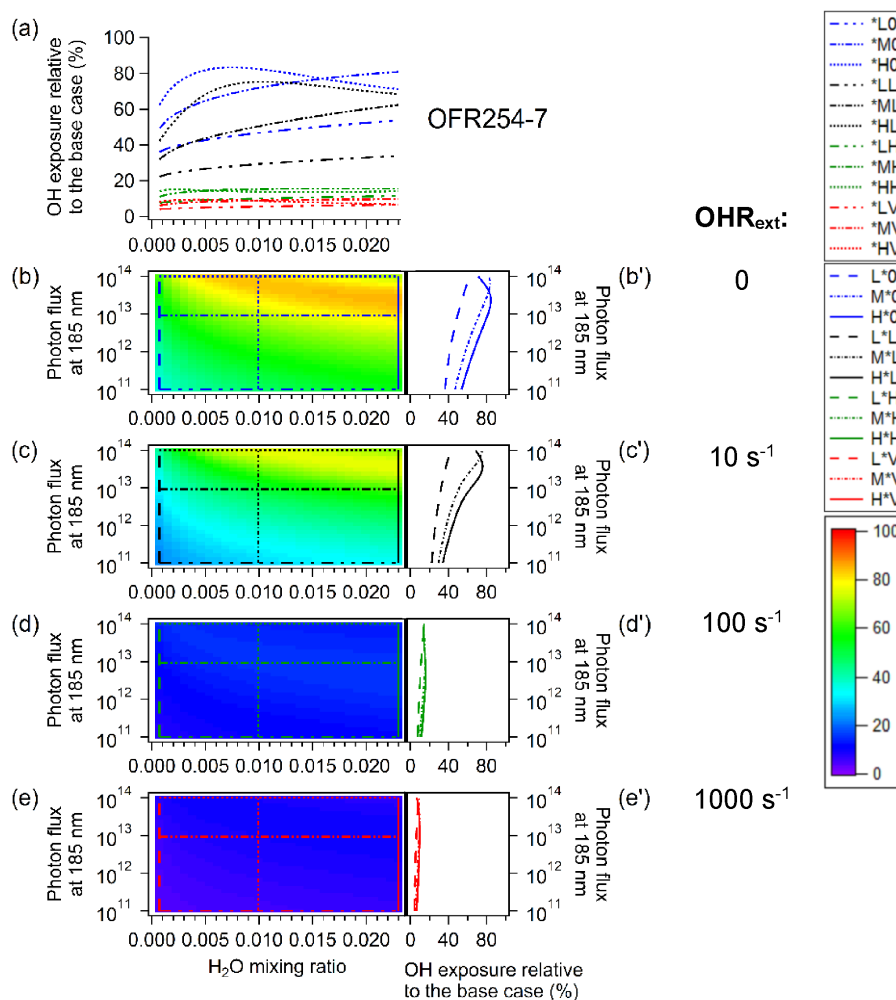


Figure 8. Percentage of OH exposure in OFR254-7 to the base case (OFR254-70) vs. the same parameters and in the same format as Fig. 2f–j, g'–j'.

nor fraction at residence times > 350 s, and hence OH_{exp} in good agreement with the plug-flow results is observed even at high H₂O, high UV, and very high OHR_{ext}.

Note that the differences between the plug-flow and Lambe-RTD OH_{exp}^{MATH} for OFR185 at high H₂O, UV, and OHR_{ext} do *not* imply a poor performance of the plug-flow model. During the residence time > 350 s, OH is ~ 10 times higher than at the average residence time in Case HHV. However, at the same time, the external OH reactant is almost completely destroyed so that OH_{exp} in this period of time is irrelevant in terms of chemical processing of the external OH reactant. The ultimate goal of using OFRs is to oxidize external OH reactants (e.g., VOCs) rapidly. Therefore, in the case of a large part of OH_{exp} not being used for external OH reactant oxidation, it is better to consider the OH_{exp} that accounts for the external OH reactant oxidation rather than the total OH_{exp}^{MATH}. Therefore, we compare OH_{exp} estimated from the decay of an external OH reactant (SO₂ in

this study, i.e., the experimental observable of the ratio of exit to intake concentration) calculated using the models with RTD (OH_{exp,RTD}^{SO₂}) to that in the plug-flow model (which is mathematically identical to OH_{exp,PF}) (Fig. 9b). Both types of OH_{exp} also compare generally well. Almost all cases of laminar RTD are within a factor of 2 of plug flow (Fig. S11), and the Lambe RTD cases deviating from OH_{exp,PF} by a factor > 2 are only a few percent (Table S1 in the Supplement).

With both OH_{exp,RTD}^{MATH} and OH_{exp,RTD}^{SO₂} introduced, the difference between them can be assessed. In no case is the former smaller than the latter (Figs. 10 and S12). When OH_{exp} is low, both types of OH_{exp} tend to be identical, while OH_{exp,RTD}^{SO₂} becomes significantly lower than OH_{exp,RTD}^{MATH} when SO₂ is significantly consumed by OH (at OH_{exp} > 10¹¹ molecules cm⁻³ s). For example, when half SO₂ is consumed, OH_{exp,RTD}^{SO₂} (LB stands for the Lambe RTD) in OFR185 is ~ 30–70 % lower than OH_{exp,RTD}^{MATH}. If SO₂ is

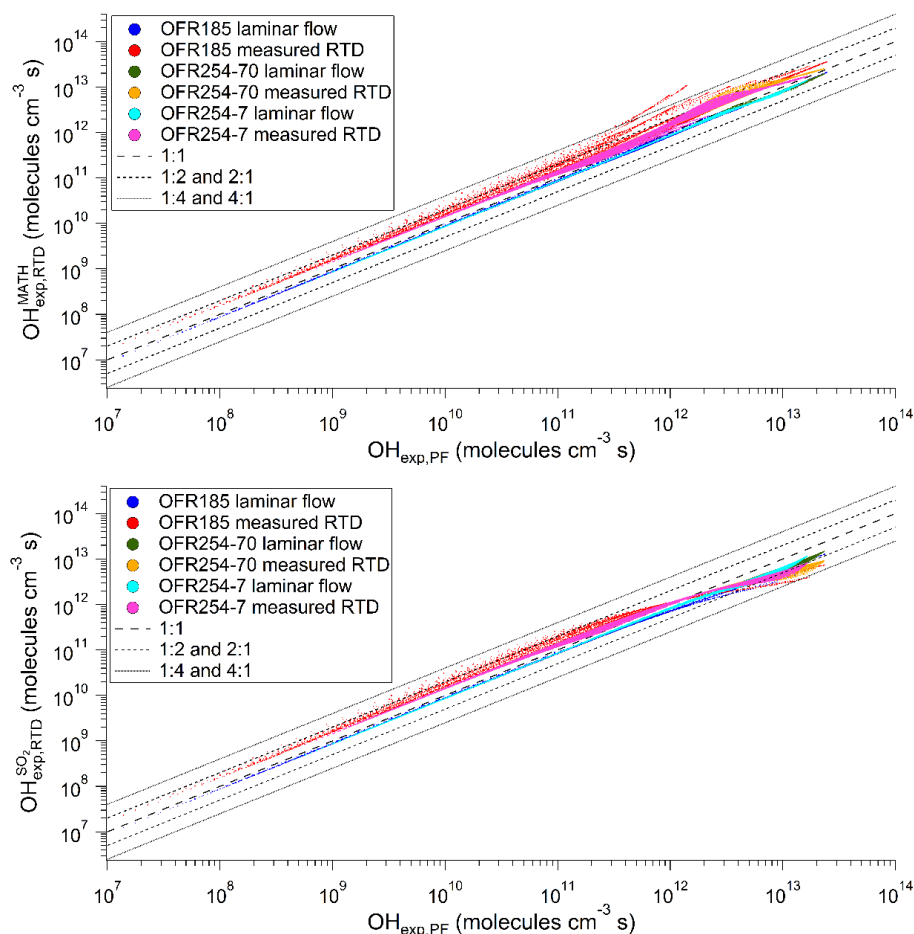


Figure 9. OH exposures calculated from direct integration ($\text{OH}_{\text{exp,RTD}}^{\text{MATH}}$, upper) and estimated from SO_2 decay ($\text{OH}_{\text{exp,RTD}}^{\text{SO}_2}$, lower) for the models with residence time distributions vs. those for the plug-flow model ($\text{OH}_{\text{exp,PF}}$). Note that for the plug-flow model both OH_{exp} definitions (MATH and SO_2) always have the same value, and thus that superscript is not used). The 1 : 1, 1 : 2, 2 : 1, 1 : 4 and 4 : 1 lines are also shown for comparison. For each type of RTD, 3600 (2700), 28 800 (27 900), and 28 800 (27 900) datapoints are shown in the upper (lower) panel for OFR185, OFR254-70, and OFR254-7, respectively.

nearly completely destroyed, $\text{OH}_{\text{exp,RTD}}^{\text{SO}_2}$ can be >5 times lower than $\text{OH}_{\text{exp,RTD}}^{\text{MATH}}$. The reason why significant SO_2 consumption can make a difference is that both the laminar and Lambe RTDs have a large portion of the flow with shorter-than-the-average residence time, which results in some parcels of air to passing through the reactor with little SO_2 reacting with OH, despite the large average OH_{exp} for the reactor. In the case of significant SO_2 consumption, the consumed SO_2 is also significantly less than that calculated from $\text{OH}_{\text{exp,RTD}}^{\text{MATH}}$. As a result, $\text{OH}_{\text{exp,RTD}}^{\text{SO}_2}$, estimated from consumed SO_2 , is lower than $\text{OH}_{\text{exp,RTD}}^{\text{MATH}}$. This suggests that $\text{OH}_{\text{exp,RTD}}^{\text{MATH}}$ may be significantly underestimated using a tracer in the OFR. On the other hand, $\text{OH}_{\text{exp,RTD}}^{\text{MATH}}$ may not be an appropriate measure of the photochemical aging of precursors since much of the periods that some air experiences high exposures may have little overlap with the presence of the precursors. Although we believe that SO_2 is generally

a better surrogate for OHR_{ext} decay than primary VOCs as discussed above, using SO_2 as a surrogate is still a source of uncertainty. For this reason, for the most accurate estimation of photochemical aging relevant to a given OFR study, we recommend using the species under study to estimate it when possible, rather than using an additional tracer with a very different lifetime, as used in some literature studies.

3.6 Summary of the relationship between OH suppression and OH reactivity

In this section we summarize modeled OH suppressions in a large variety of cases in the space of examined physical conditions, and rationalize these OH suppressions in terms of parameters relevant to OH reactivity. In Sects. 3.6.1 and 3.6.2 we relate OH suppression to $\text{OHR}_{\text{int}}/\text{OHR}_{\text{tot}}$ in a more theoretical and fundamental manner. In Sect. 3.6.3 we use $\text{OHR}_{\text{O}_3}/\text{OHR}_{\text{ext}}$ for a more phenomenological and practi-

cal discussion, as both OHR_{O₃} and OHR_{ext} are experimental observables.

3.6.1 Relationship between OH suppression and OHR_{int} / OHR_{tot}

OHR_{tot} in OFRs is of the order of 1–10³ s⁻¹, leading to OH lifetimes of ~ 10⁻³–1 s, which is orders of magnitude shorter than the residence time of OFRs, ~ 10² s. Thus we can apply the steady-state approximation to the analysis of OH concentration, i.e.,

$$P = L = \text{OH} \times \text{OHR}_{\text{tot}} = \text{OH} \times (\text{OHR}_{\text{int}} + \text{OHR}_{\text{ext}}), \quad (4)$$

where P and L are the production and loss rates of OH, respectively. This equation can be rearranged as

$$\text{OH} = P / (\text{OHR}_{\text{int}} + \text{OHR}_{\text{ext}}). \quad (5)$$

In the absence of OHR_{ext}, OH is

$$\text{OH}_0 = P_0 / \text{OHR}_{\text{int},0}, \quad (6)$$

where the subscripts denote the case of OHR_{ext} = 0. Therefore, the measure of OH suppression used in the manuscript, fraction of remaining OH after suppression is

$$\begin{aligned} \text{rOH}_{\text{exp}} &= \frac{\text{OH}}{\text{OH}_0} = \frac{P}{P_0} \times \frac{\text{OHR}_{\text{int},0}}{\text{OHR}_{\text{tot}}} = \frac{P}{P_0} \times \frac{\text{OHR}_{\text{int},0}}{\text{OHR}_{\text{int}}} \\ &\quad \times \frac{\text{OHR}_{\text{int}}}{\text{OHR}_{\text{tot}}}. \end{aligned} \quad (7)$$

If P and OHR_{int} did not change when OHR_{ext} is added, rOH_{exp} would be

$$\text{rOH}_{\text{exp}} = \frac{\text{OHR}_{\text{int}}}{\text{OHR}_{\text{tot}}}. \quad (8)$$

We refer to this equation as the “simplified model” below. As shown in Fig. 4, OHR_{int,0} varies on the range 1–100 s⁻¹ over the very wide range of conditions explored here, with typical values of the order of 20 s⁻¹. Thus based on the simplified model it is expected that OH suppression will be significant when OHR_{ext} > 20 s⁻¹. We note that the relevant OHR values are the averages over the reactor residence time.

We compare rOH_{exp} vs. OHR_{int} / OHR_{tot} for the simplified and full models in Fig. 11a. Results from the full model are close to those of the simplified model, with most datapoints within a factor of 2. This demonstrates that the OH suppression results have a solid theoretical foundation. The ratios of full to simplified model OH suppressions in OFR185, OFR254-70, and OFR254-7 have geometric means of 0.51, 1.02, and 0.90, respectively, and uncertainty factors (see Sect. 2.3.1) of 1.27, 1.07, and 1.26, respectively. The differences between the full and the simplified models are thus comparable to the uncertainties due to chemical kinetic parameters.

In addition, deviations from the analytical prediction line can also be explained as follows.

- i. OFR185 datapoints are systematically below the simplified model. This results from OHR_{int,0} / OHR_{int} being lower than 1 (Fig. S14), because OHR_{int} increases as the external OH reactant converts OH to HO₂. P/P_0 is always ~ 1 (Fig. S13) while OHR_{int,0} / OHR_{int} is roughly 0.5 on average, leading to a ratio of ~ 0.5 between the full and simplified model values.
- ii. OFR254 points at low H₂O and/or UV lie across the simplified model prediction. Since, at low H₂O and/or UV, the dominant contribution to both P and OHR_{int} is from O₃, P and OHR_{int} are both very close to the value at OHR_{ext} = 0 (Figs. S13 and S14), leading to very small deviations from the simplified model prediction. However, the right part of each strip of datapoints in Fig. 11a deviate from the simplified model more significantly. These points correspond to high H₂O and/or UV conditions, where both P and OHR_{int} are higher than P_0 and OHR_{int,0}. P is elevated (by up to ~ 50 %) compared to P_0 , as HO₂, which can be recycled to OH by O₃, is efficiently produced during the destruction of external OH reactant. OHR_{int} is more elevated (by a factor up to ~ 10) compared to OHR_{int,0}, as not only HO₂ increases, but also H₂O₂. Thus, the overall product of P/P_0 and OHR_{int,0} / OHR_{int} is < 1 at high H₂O and UV, leading to negative deviations of the corresponding datapoints from the simplified model prediction. Thus in those cases the simplified model *underestimates* OH suppression.

Considering the minor and explainable deviations, we conclude that OH suppression can be estimated within a factor of ~ 2–3 as OHR_{int} / OHR_{tot}.

3.6.2 Model-estimated OH suppression for literature studies

To illustrate the range of OH suppressions that may have been present in previous OFR studies, we estimate rOH_{exp} and OHR_{int} / OHR_{tot} in several literature OFR experiments with our model. We strive to include experiments that span a range of different precursors and conditions. We obtained experimental conditions (relative humidity, residence time, OHR_{ext} etc.) from the relevant papers. However, as no information of UV can be found in the selected literature studies, UV is estimated according to literature OH_{exp}. We emphasize that as long as its impact is carefully taken into account, OH suppression is not a “problem” but an “expected feature” of OFR experiments. Only when OH suppression is not taken into account, e.g., when OH_{exp} calibration experiments use OHR_{ext} that are very different from the experiments of interest, it can result in significant errors in the estimated OH_{exp}. The literature experiments simulated here include two series of OFR254 laboratory experiments with various precursors (Kang et al., 2011; Lambe et al., 2011b), two series of OFR254 laboratory experiments with specific pre-

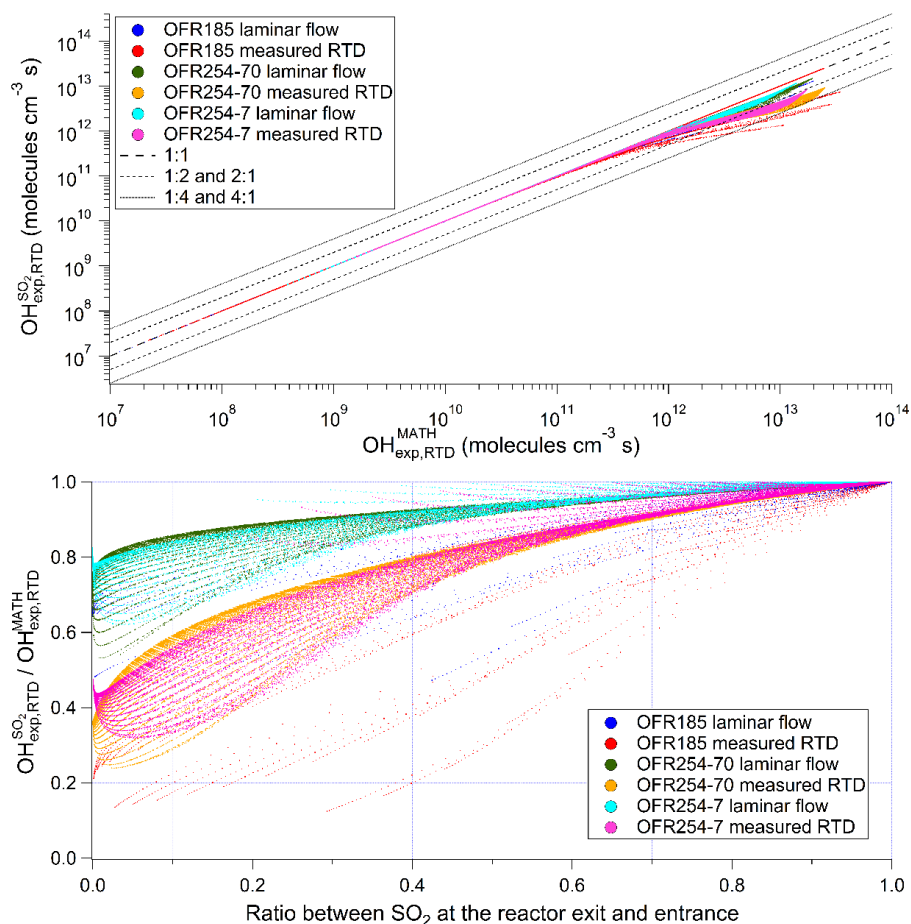


Figure 10. (upper) OH exposures estimated from SO₂ decay in the models with residence time distributions ($\text{OH}_{\text{exp,RTD}}^{\text{SO}_2}$) vs. those calculated from direct integration for the models with residence time distributions ($\text{OH}_{\text{exp,RTD}}^{\text{MATH}}$). The 1 : 1, 1 : 2, 2 : 1, 1 : 4 and 4 : 1 lines are also shown for comparison. (lower) Ratios between the two types of OH exposures as a function of the fractional consumption of SO₂ in the reactor. For each type of RTD, 2700, 27 900, and 27 900 datapoints are shown for OFR185, OFR254-70, and OFR254-7, respectively.

cursors, i.e., JP-10 (tricyclo[5.2.1.0^{2,6}]decane) and isoprene, respectively (Lambe et al., 2012, 2015), and a source study in an urban tunnel using OFR185 (Tkacik et al., 2014). As isoprene reacts very rapidly with OH and may not be well surrogated by SO₂ even when including the OH reactivity of its oxidation products, its chemistry is thus modeled with the semi-explicit scheme in Krechmer et al. (2015). Note that the OH suppressions in the experiments are obtained from the model using the best available information or estimates of the experimental conditions.

The results of the plug-flow model and the model with the RTD reported in Lambe et al. (2011a) are in generally good agreement (Fig. 11a). Both of them suggest that some degree of OH suppression played a role in all investigated previous studies, which is consistent with most of the experimental data available for those experiments. The range of the remaining OH after suppression in the JP-10 experiments of Lambe et al. (2012) is estimated by the model to be ~60–

70 %, in reasonable agreement with the measured values of ~50–90 %.

Next we compare the remaining OH reported for the calibration experiments of Tkacik et al. (2014) using NO vs. a modeled range. The comparison is shown in Fig. S15. The model reproduces well the OH suppression at lamp voltages of 75 and 110 V, while it overestimates the percentage of remaining OH (i.e., it *underestimates* the OH suppression) at 45 V. The latter lamp voltage is near the threshold of lamp emission and where UV flux is most uncertain and differences between individual lamps can be greatest, so the larger uncertainty in UV may be responsible for the observed differences. If UV at 45 V is reduced by a half, modeled OH suppression is indeed in very good agreement with the measurements.

The modeled OH remaining for the tunnel study (~5–50 %, Fig. 11a) is lower than for the calibration cases. Tkacik et al. (2014) only used NO as external OH reactant in their OH_{exp} calibration experiments, while our modeled cases also

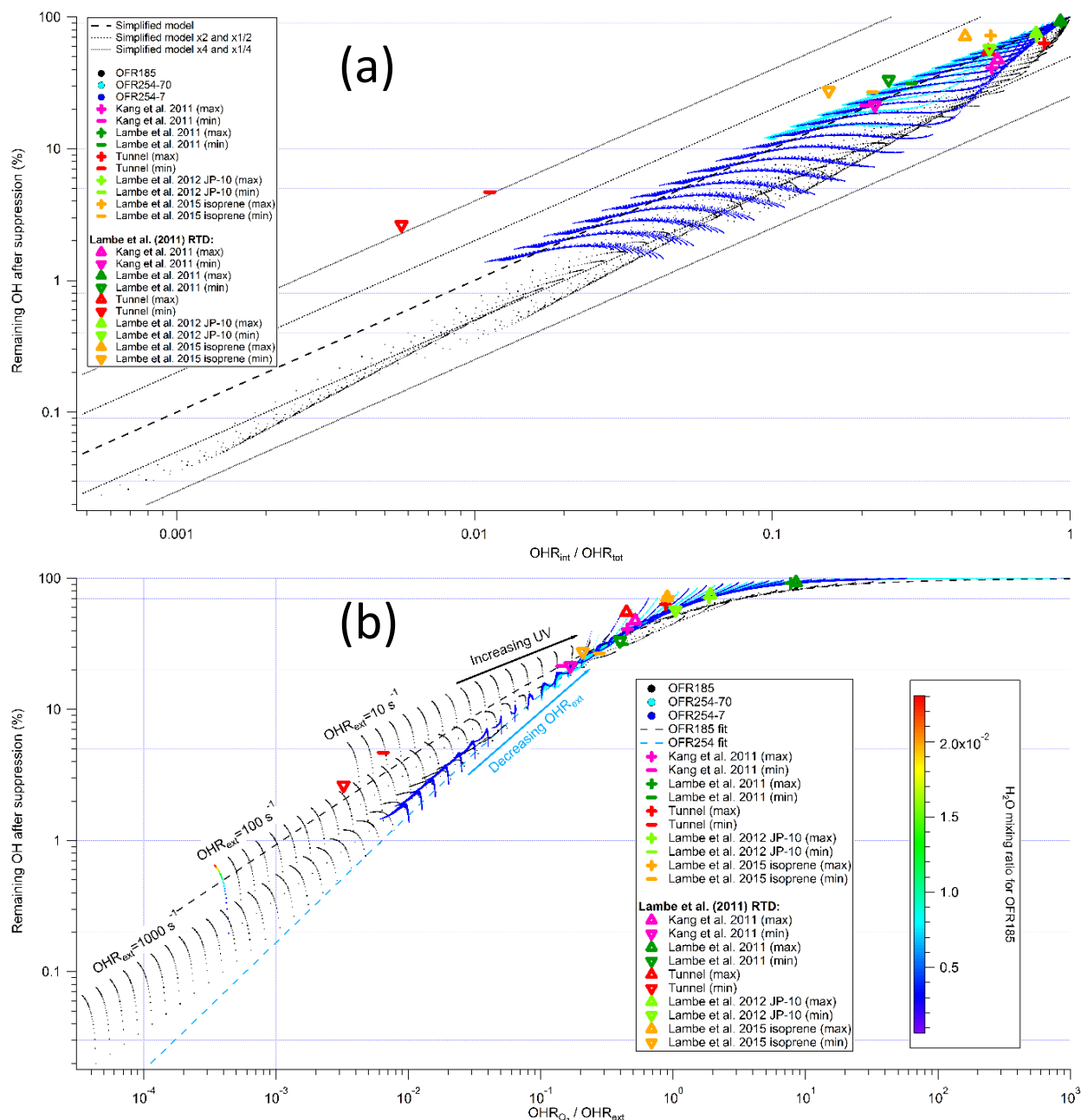


Figure 11. (a) Percentage of remaining OH after suppression in OFR185 (black dot), OFR254-70 (cyan dots), and OFR254-7 (blue dots) vs. the ratio between internal and total OH reactivities. The “simplified model” (Eq. 8) prediction as well as lines at x2, x4, x1/2, and x1/4 of the simplified model are also shown for comparison. The estimated ranges for laboratory experiments (Kang et al., 2011; Lambe et al., 2011b, 2012, 2015) and a source study in an urban tunnel Tkacik et al., 2014) are also shown. These ranges are estimated by the models with plug flow and with the Lambe et al. (2011a) residence time distribution according to the experimental conditions in these studies. The lower limit of the percentage of remaining OH after suppression in the tunnel study is notably above the simplified model, since the large amount of NO_x in that case destroys a significant fraction of the internal OH reactants (e.g., O₃, HO₂, and OH), leading to $OHR_{int,0} / OHR_{int}$ much higher than 1, while the major contribution of H₂O photolysis to both P and P_0 leads to P/P_0 close to 1. (b) Percentage of remaining OH after suppression in OFR185 (black dot), OFR254-70 (cyan dots), and OFR254-7 (blue dots) vs. the ratio of OH reactivity from O₃ to external OH reactivity. The fit curves for OFR185 (black dash) and OFR254 (light blue dash) are shown. The estimated ranges for laboratory experiments (Kang et al., 2011; Lambe et al., 2011b, 2012, 2015) and a source study in an urban tunnel (Tkacik et al., 2014) are also shown. These ranges are estimated by the models with plug flow and with the Lambe et al. (2011a) residence time distribution according to the experimental conditions in these studies (see text). The three series of OFR185 datapoints corresponding to $OHR_{ext} = 10$, 100, and 1000 s⁻¹ are respectively labeled. A strip of OFR185 datapoints are colored by H₂O mixing ratio.

include CO (measured in Tkacik et al. (2014) but neglected when OHR_{ext} was considered) and VOCs (estimated from their ratios to CO according to Borbon et al. (2013)), which also comprise a large fraction of OHR_{ext}. NO_x is rapidly oxidized to HNO₃ in OFRs (Li et al., 2015) consuming a single OH in the process, and hence is less effective at suppressing OH during most of the residence time. CO and VOCs more effectively reduce OH over the entire residence time, since CO reacts with OH slowly, and many generations of oxidation products of the initial VOCs continue to react with OH. Therefore, although CO and VOCs may appear less important in suppressing OH than NO_x in terms of initial OHR_{ext}, they are actually more important in terms of effective OH reduction or effective OHR_{ext} (averaged over the residence time). If we exclude CO and VOCs from the modeled tunnel cases, the modeled percentage of remaining OH will be ~10–80%, which is consistent with the measured range in the calibration experiments with pure NO in the tunnel study (~20–95%; Lambe, 2015).

Thus the OH_{exp} predicted by the model, which had already been validated by Li et al. (2015), results in OH suppression predictions that are also consistent with most previous literature measurements. There is however one case for which a disagreement between modeled and measured OH suppressions is observed: the isoprene experiments in Lambe et al. (2015). This is observed despite taking into account the expected decrease in OHR_{ext} with OH_{exp} as noted above. Our model suggests a percentage of remaining OH after suppression from ~30 to ~70% in these experiments, while Lambe et al. (2015) reported no measurable OH suppression (based on measurements using SO₂, not isoprene). If OH production is about constant as shown above (Fig. S13), it is virtually impossible to explain (e.g., using Eq. 7) an observation of OH concentration being constant when its lifetime is reduced by a large factor by high OHR_{ext}. One complexity of isoprene chemistry is OH recycling. However, we already include an OH recycling of 6.3% (Liu et al., 2013) for the primary oxidation of isoprene and a full OH recycling for the conversion of isoprene-derived hydroxyhydroperoxides (ISOPOOH) into epoxydiols (IEPOX) (Paulot et al., 2009) in the reaction scheme. The magnitude of the effect of OH recycling of other reactions of isoprene and its oxidation products is much too small to explain the observed deviations. For OH suppression to be negligible, OH recycling would need to be ~100% for isoprene and for many subsequent generations of its oxidation products, which is very unrealistic. Although isoprene chemistry is not known in complete detail, we cannot explain such a large deviation between measurements and model predictions using any known or plausible chemical processes.

In addition, the effect of non-plug flow does not explain the model-measurement discrepancy. As shown in Fig. S16, OH suppression in the literature studies estimated by the model with the Lambe et al. (2011a) RTD is very close to that estimated by the plug-flow model, regardless of what is con-

sidered as OH_{exp} in the non-plug-flow model (see Sect. 3.5) and whether UV is fixed to the value estimated in the plug-flow model.

In summary, the reasons for the model-measurement discrepancy for the case of isoprene remain unclear, and may include contributions from uncertain isoprene chemistry in the model or other model and measurement uncertainties. We suggest that the OH oxidation of isoprene in OFRs be investigated further with a combined model/measurement approach, over a wide range of experimental conditions (initial isoprene, H₂O, and UV) and with direct measurements of isoprene and its oxidation products. If a complete lack of OH suppression is consistently observed in future experiments, its explanation may be of great interest to understand the chemistry of isoprene oxidation.

3.6.3 Relationship between OH suppression and OHR_{O₃} / OHR_{ext}

Although the relationship between rOH_{exp} and OHR_{int} / OHR_{tot} makes clear the origin of OH suppression, neither OHR_{int} nor OHR_{tot} can be easily measured or estimated, because of the short-lived radicals comprising a large fraction of OHR_{int}, i.e., HO₂ and OH, and the difficulty of measuring H₂O₂. To provide a more practical method to estimate rOH_{exp}, we show another consistent relationship between rOH_{exp} and a quantity related to OHR.

In the discussions above, we have seen several cases where OH suppression in OFR254 is regulated by both O₃ and OHR_{ext}. At OHR_{ext} ≤ 100 s⁻¹ in OFR254-70 (OHR_{O₃} = 101 s⁻¹), O₃-promoted interconversion of HO_x is highly active and a comparable or smaller amount of OHR_{ext} cannot significantly perturb this recycling. Therefore, OH concentration remains relatively stable with increasing OHR_{ext}, leading to negligible or small OH suppression. When OHR_{ext} is ≫ 100 s⁻¹ in OFR254-70, the steady state between OH and HO₂ due to their interconversion is overwhelmingly shifted toward HO₂ by the large amounts of external OH reactant. In other words, OH is strongly suppressed. In OFR254-7 (OHR_{O₃} = 10 s⁻¹), the HO_x interconversion is less resilient to OHR_{ext}. A 100 s⁻¹ OHR_{ext} can already greatly affect this interconversion and lead to strong OH suppression.

These facts suggest that OH suppression in OFR254 depends on OHR_{int} due to O₃, OHR_{O₃}, relative to OHR_{ext}. We thus investigate the dependence of OH suppression on the ratio OHR_{O₃} / OHR_{ext}. Such a relationship is summarized in Fig. 11b for not only OFR254 (OFR254-70 and OFR254-7), but also OFR185, as the resilience of OH_{exp} to OHR_{ext} in OFR185 also stems from O₃-promoted HO_x recycling.

OH suppression is negligible if OHR_{O₃} / OHR_{ext} ≫ 1. As this ratio decreases towards 1, we observe a regime change, where OH_{exp} begins to significantly decrease compared to the cases without OHR_{ext}. After that, the percentage of remaining OH after suppression (rOH_{exp}, i.e., the per-

centage of OH relative to that in the case with $\text{OHR}_{\text{ext}} = 0$) exhibits a nearly exponential decrease with decreasing $\text{OHR}_{\text{O}_3} / \text{OHR}_{\text{ext}}$. This trend can be fitted by a sigmoid of $\log(\text{OHR}_{\text{O}_3} / \text{OHR}_{\text{ext}})$, i.e.,

$$r\text{OH}_{\text{exp}} = \frac{100}{1 + \exp\left(\frac{x_0 - \log(\text{OHR}_{\text{O}_3} / \text{OHR}_{\text{ext}})}{s}\right)}, \quad (9)$$

where x_0 and s are fitting parameters. s measures the steepness of the increasing part of the curve: the smaller s , the steeper the curve. For OFR185 $x_0 = -0.021$ and $s = 0.638$, while for OFR254 (fitted from both OFR254-70 and OFR254-7 data) $x_0 = -0.155$ and $s = 0.445$. The steeper OH suppression for OFR254 reflects a generally faster decrease of remaining OH after suppression with decreasing O_3 and/or increasing OHR_{ext} . In other words, in cases with significant OH suppression, OH in OFR254 is usually more suppressed than in an OFR185 at the same $\text{OHR}_{\text{O}_3} / \text{OHR}_{\text{ext}}$, as shown in Fig. 11b. This can be explained by the fact that for the same value of $\text{OHR}_{\text{O}_3} / \text{OHR}_{\text{ext}}$, OHR_{O_3} and OHR_{ext} in OFR185 are usually smaller than in OFR254, because O_3 in OFR185 generally cannot be as high as that injected in OFR254 unless it was used at very high UV.

This relationship between OH suppression and $\text{OHR}_{\text{O}_3} / \text{OHR}_{\text{ext}}$ holds not only for SO_2 as an OH reactant, but also for real primary VOCs and their oxidation intermediates. We observe the same trend for the cases with external OH reactant surrogates reacting with OH at 0 (constant $\text{OHR}_{\text{ext}} = 1.8 \times 10^{-10} \text{ cm}^3 \text{ molecules}^{-1} \text{ s}^{-1}$ (collision rate) as for the base case with SO_2 (Fig. S17). For both OFR185 and OFR254, datapoints of all external OH reactant surrogates in the whole explored H_2O , UV, and OHR_{ext} range are in a very narrow corridor showing the above-mentioned trend. In the case of a faster OH reactant decay, average OHR_{ext} is lower, which leads to both higher $r\text{OH}_{\text{exp}}$ and $\text{OHR}_{\text{O}_3} / \text{OHR}_{\text{ext}}$. The point corresponding to this case shifts toward upper right in Fig. S17, but is still located in the corridor. We can similarly rationalize the case of a slower OH reactant decay. The results in Fig. S17 suggest that even in the case of real VOC oxidation in OFR, where OH reactants are various and OHR_{ext} variation is highly complex, OH suppression still follows the relationship proposed herein.

We also estimate the ranges of $r\text{OH}_{\text{exp}}$ and $\text{OHR}_{\text{O}_3} / \text{OHR}_{\text{ext}}$ of the previous OFR experiments discussed above (Fig. 11b). All estimated values of $r\text{OH}_{\text{exp}}$ vs. $\text{OHR}_{\text{O}_3} / \text{OHR}_{\text{ext}}$ of these experiments follow this relationship well. Most of the estimated values fall into the regime where OH suppression is significant (estimated remaining OH range $\sim 5\text{--}70\%$). This suggests that unless OH_{exp} is calibrated during the relevant experiments by measuring the decay of a reactant, O_3 and OHR_{ext} need to be known to estimate the extent of OH suppression. Using OH_{exp} measured under low OHR_{ext} conditions for experiments at

high OHR_{ext} can lead to more than a 1-order-of-magnitude error in the estimated OH_{exp} , even if UV and H_2O are kept constant.

Note that the $r\text{OH}_{\text{exp}}$ ranges estimated above are based on SO_2 (reaction rate constant with OH: $9.185 \times 10^{-13} \text{ cm}^3 \text{ molecules}^{-1} \text{ s}^{-1}$) as VOC surrogate. Employing a VOC decaying more slowly than SO_2 (e.g., CH_4) leads to similar OH suppression, as shown by the case with constant OHR_{ext} (Sect. 3.4.2). However, in the case of a VOC decaying faster than SO_2 , some significant discrepancies may arise. Assuming a VOC consumed by OH at $1 \times 10^{-11} \text{ cm}^3 \text{ molecules}^{-1} \text{ s}^{-1}$ without downstream oxidation, which is already unrealistic, we estimate that the difference in average OHR_{ext} between this case and the SO_2 case can be up to ~ 10 (with an OH_{exp} larger than $3 \times 10^{12} \text{ molecules cm}^{-3} \text{ s}^{-1}$, destroying almost all OH reactant in both cases). Then the resulting difference in $r\text{OH}_{\text{exp}}$ can be estimated by Eq. (9). $r\text{OH}_{\text{exp}}$ in this case can be up to ~ 5 and ~ 10 times higher than in the SO_2 case. However, these larger differences occur only if the initial OHR_{ext} is high enough to cause significant OH suppression, and OH_{exp} is high enough to consume most OH reactant. Under most conditions, the differences between the two cases are within a factor of 2 and 3 for OFR185 and OFR254, respectively.

3.7 Equations for estimating OH_{exp} in OFR254

Li et al. (2015) discussed the usefulness of an estimation equation for OH_{exp} for OFR, for both laboratory and especially field experiments. An equation was reported for OFR185 in which OH_{exp} is estimated from H_2O and OHR_{ext} inputs and O_3 output ($\text{O}_{3,\text{out}}$), with the latter parameter serving as a surrogate of UV intensity (Li et al., 2015). The full equation is shown as below

$$\begin{aligned} \log \text{OH}_{\text{exp}} = & 26.89 + \left(-1.7629 - 1.2947 \cdot \text{OHR}_{\text{ext}}^{0.076549} \right. \\ & \left. + 0.14469 \cdot \log \text{O}_{3,\text{out}} \cdot \text{OHR}_{\text{ext}}^{0.046} \right) \\ & \cdot \log \text{O}_{3,\text{out}} + \log \text{H}_2\text{O}. \end{aligned} \quad (10)$$

In this study, we expand upon the previous work by deriving estimation equations for OFR254.

3.7.1 Estimation equation for OH_{exp} as a function of H_2O , UV, OHR_{ext} , and $\text{O}_{3,\text{in}}$

As discussed in the previous subsection, besides H_2O , UV, and OHR_{ext} , the amount of initially injected O_3 in OFR254 ($\text{O}_{3,\text{in}}$) also has a major impact on OH_{exp} . First, we derive an estimation equation of OH_{exp} as a function of these four variables based on all OH_{exp} datapoints that we calculated in the explored range of H_2O ($0.0007\text{--}0.023$, 30 linearly evenly spaced points), UV ($4.2 \times 10^{13}\text{--}8.5 \times 10^{15} \text{ photons cm}^{-2} \text{ s}^{-1}$ at 254 nm, 30 points corresponding to exponentially evenly spaced points of UV at

185 nm between 10^{11} – 10^{14} photons $\text{cm}^{-2} \text{s}^{-1}$), and OHR_{ext} (1 point at 0 s^{-1} and 31 exponentially evenly spaced points in the range of 1 – 1000 s^{-1}), as well as the range of $\text{O}_{3,\text{in}}$ between 7 and 70 ppm (11 exponentially evenly spaced points). In total 316 800 datapoints obtained from the base case of the model (non-HO_x-destructive SO₂ as surrogate of external OH reactant) are used to derive the following estimation equation:

$$\log \text{OH}_{\text{exp}} = a + b_1 \log \text{H}_2\text{O} + b_2 (\log \text{H}_2\text{O})^2 + c_1 \log \text{UV} + c_2 (\log \text{UV})^2 \quad (11)$$

$$- \log \left(1 + \exp \left(\frac{d - \log (\text{O}_{3,\text{in}} / \text{OHR}_{\text{ext}})}{e} \right) \right), \quad (12)$$

where H₂O (water mixing ratio) is unitless, and OH_{exp}, UV, OHR_{ext}, and O_{3,in} are in molecules $\text{cm}^{-3} \text{ s}$, photons $\text{cm}^{-2} \text{ s}^{-1}$, s^{-1} , and ppm, respectively. a , b_1 , b_2 , c_1 , c_2 , d , and e are fitting parameters. The equation is composed of a part of OH_{exp} at 0 OHR_{ext} (first row) and a part representing OH suppression (second row), which is very similar to Eq. (9). Considering the non-linearity of the model response, we use two terms for each variable that has major influence on OH_{exp} in the case without OHR_{ext}, i.e., H₂O and UV. The fitting parameters (Table S2) are obtained by fitting Eq. (11) to the OH_{exp} model results that we calculate using the model in the variable space spanned by H₂O, UV, OHR_{ext}, and O_{3,in}. Figure 12a shows the comparison between OH_{exp} calculated from the full model and estimated by Eq. (11). Most estimated OH_{exp} datapoints are within a factor of 2 from the full model OH_{exp}. The mean absolute value of the relative deviation is 15 % (Fig. 12a), which is smaller than the parametric uncertainty of the model discussed above. The satisfactory performance of Eq. (11) demonstrates its applicability to OFR254 under a very wide range of conditions.

However, this applicability may be constrained by the UV flux, the variable in Eq. (11) that is most difficult to measure. For OFRs using the same lamps and power supplies as in our laboratory, we provide with a UV-flux to lamp voltage relationship (Fig. S18) that allows estimating UV from lamp voltage. This equation is based on UV flux vs. lamp setting relationship reported by Li et al. (2015), and the lamp setting-lamp voltage relationship from our group's previous measurements. This result allows the application of Eq. (11) to PAM OFRs and others using the same lamps. However, the fluxes reported in Li et al. represent the average or “effective” flux throughout the reactor, and the output of individual Hg lamps may vary depending on the lamp, its age and usage, and possibly its temperature. As a consequence, there is a substantial uncertainty in the UV flux estimated from lamp voltages. An alternative method to estimate OH_{exp} without using the estimated UV flux is thus desirable.

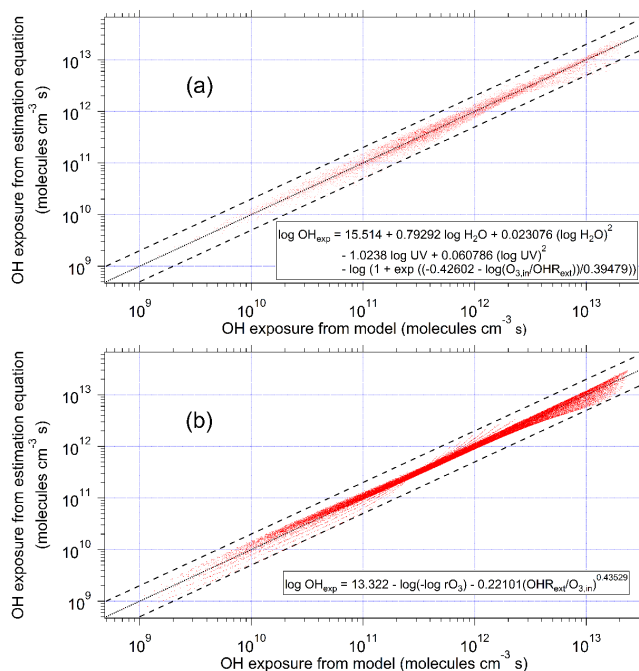


Figure 12. Comparison of OH exposure (OH_{exp}) estimated from the estimation equations, i.e., (a) Eq. (11) and (b) Eq. (12), vs. the model results. 1 : 1, 1 : 2, and 2 : 1 lines are also shown to facilitate the comparison.

3.7.2 Estimation equation for OH_{exp} as a function of $r\text{O}_3$, OHR_{ext}, and O_{3,in}

The OH_{exp} estimation equation proposed by Li et al. (2015) for OFR185 avoided an explicit dependence on UV by using instead O₃ as its surrogate, since in OFR185 this species is only formed by the 185 nm radiation. We follow a similar approach to derive an alternative estimation equation for OH_{exp} in OFR254 in which the logarithm of the ratio of the output to input O₃ ($\log r\text{O}_3 = \log (\text{O}_{3,\text{out}} / \text{O}_{3,\text{in}})$) is used as a surrogate of UV, as well as H₂O, since both photons and HO_x produced from H₂O destroy O₃. OH_{exp} can then be expressed as a function of only $r\text{O}_3$, OHR_{ext}, and O_{3,in}:

$$\log \text{OH}_{\text{exp}} = a - \log (-\log r\text{O}_3) + b (\text{OHR}_{\text{ext}} / \text{O}_{3,\text{in}})^c, \quad (13)$$

where a – c are fitting parameters. Their values are reported in Table S2. Obviously, Eq. (12), with only three input variables and three parameters, is much simpler than Eq. (11). Furthermore, the mean absolute value of the relative deviation between OH_{exp} estimated by Eq. (12) and computed by the full model is only 9 %, and the scatter in the relationship is substantially smaller than for Eq. (11) (Fig. 12b). O₃ can be easily monitored in OFR254 experiments at both the entrance and the exit of the OFR with a single O₃ analyzer and a switching valve system. Therefore, we recommend measuring both O₃ input and output concentrations in OFR254 experiments to more simply and accurately estimate OH_{exp}.

Note that a good experimental determination of rO_3 requires that a measurable amount of O_3 is destroyed, but also that some O_3 still remains at the reactor output. We estimate this range as corresponding to rO_3 between 0.05 and 0.95. However, $rO_3 > 0.95$ (i.e., only $< 5\%$ of O_3 , in is destroyed in the OFR) only occurs under low H_2O and/or UV conditions, where OH_{exp} is also very low and may be of limited experimental interest, while $rO_3 < 0.05$ occurs rarely, i.e., only at the highest H_2O and UV that we explored. For experiments where rO_3 is very low or close to 1, Eq. (11) can be applied to estimate OH_{exp} .

The good performance of Eq. (12) can be explained by a key relationship between OH_{exp} and rO_3 . Note that the last term in Eq. (12) is minor: $b(OHR_{ext}/O_{3,in})^c$ generally ranges 0.5–1, while $-\log rO_3$ spans orders of magnitude. Thus, $\log OH_{exp}$ is approximately proportional to $\log(-\log rO_3)$, which already captures effects of both H_2O and UV, as well as partial effects of OHR_{ext} and $O_{3,in}$. The last term in Eq. (12) can be regarded as a minor correction. Using the destruction of O_3 is conceptually similar to estimating OH_{exp} by measuring the decay of conventional OH reactants, e.g., SO_2 and CO . To estimate OH_{exp} , we utilize the relationship that the loss of reactant molecules is proportional to OH_{exp} and their rate constant. However, when O_3 destruction is used as the basis for OH_{exp} estimation, the relationship is somewhat different. An approximate proportional relationship still holds between gross consumed OH and net consumed O_3 , hence also between OH_{exp} and $\log rO_3$.

Note that both estimation equations are based on SO_2 as VOC surrogate. Although not common, both equations may lead to a significant underestimation in OH_{exp} , if effective OH reactant decays significantly faster than SO_2 in an experiment. In this case, a correction factor can be estimated by Eq. (4) according to the external OH reactant decay rates, as described in Sect. 3.6.3.

We expect that the functional form of these equations will apply to OFR254 setups operated from other researchers, given the common drivers and chemistry. However the numerical values of the coefficients may vary for, e.g., reactors of different geometries. We recommend always refitting the estimation equations to data for the system of interest (e.g., using experimental VOC decay curves), and reporting them in the literature (e.g., Palm et al., 2015). We also note that the residence time is assumed as 180 s for our equations. As a first-order estimate, the OH_{exp} should be multiplied by $RT/180$, where RT is the residence time used in s. This RT correction will have an error smaller than the uncertainties in the model except under extreme cases of very short residence times or large OH suppression.

4 Conclusions

We performed a systematic modeling study of the O_x and HO_x radical chemistry in OFR185 and OFR254 as a function of H_2O mixing ratio, UV photon flux, and external OH reactivity. In general, the higher H_2O mixing ratio and UV photon flux and/or the lower external OH reactivity, the higher OH exposure in OFRs.

Active OH-to- HO_2 recycling was observed in the system and is much stronger in OFR254 with 70 ppm O_3 injected as simulated here because a large amount of injected O_3 promotes both sides of this interconversion in OFR254. Strong OH production and OH-to- HO_2 recycling due to injected O_3 leads to a greater resilience of the chemistry in OFR254 to the suppression of OH by external OH reactivity. In OFR185, OH can be $\sim 100\%$ suppressed at low H_2O mixing ratio, low UV photon flux, and high external OH reactivity, while $\sim 50\%$ OH remains in OFR254 under the same condition. However when OFR254 is used with lower input O_3 levels as done in many studies, similarly large OH suppression as in OFR185 is observed due to the inability of O_3 to recycle HO_2 to OH at a sufficient rate.

An uncertainty analysis of this chemistry based on Monte Carlo uncertainty propagation and correlation analysis was performed. The relative uncertainty of OH exposure due to uncertain rate constants and photolysis parameters is 25 % or less. The uncertainties of other key model outputs (O_3 concentration, ratio between HO_2 and OH exposures, and H_2O_2 concentration) are at most $\sim 40\%$. Compared to the dynamic range of OH exposure and O_3 concentration (3–5 orders of magnitude), these small parametric uncertainties indicate that the chemical parameters are known well enough for the purposes of OFR modeling, and that other simplifications in the model (e.g., uniform radiation field, plug flow) may contribute more to the model uncertainty. The reactions contributing the most output uncertainties were identified by uncertainty analysis. These reactions are photolysis of O_3 , O_2 , and H_2O and reactions of OH and HO_2 with themselves or some abundant species, i.e., O_3 and H_2O_2 .

We also investigated the effect of non-plug flow. Compared to the plug-flow model, applying the residence time distributions of laminar flow and that measured by Lambe et al. (2011a) results in OH_{exp} generally within a factor 2. However, OH_{exp} calculated from direct integration in the models with residence time distributions is significantly higher than that estimated from SO_2 decay in the same model, when SO_2 is significantly consumed. Considering various rate constants of reactions of precursors with OH, we thus recommend using OH_{exp} estimated from the decay of species under study, if possible, as the appropriate measure of photochemical aging in the OFR.

Switching to HO_x -destructive external OH reactivity was found to have a moderate impact on OH exposure under most conditions. At low H_2O mixing ratio, low UV photon flux, and high external OH reactivity, using HO_x -destructive ex-

ternal OH reactants instead of non-destructive ones (that regenerate HO_x) can result in a significantly lower OH exposure. Changing the identity of the external OH reactant (i.e., its rate constant of reactions with OH) while keeping the input external OH reactivity constant can result in major changes in OH exposure. Reactants with high rate constants decay quickly and reduce OHR_{ext} at later times in the reactor if corresponding products are not considered as external OH reactivity. Those reactants result in increased OH exposure.

OH suppression in OFR254 is shown to be very sensitive to the amount of injected O₃ in OFR254. This can be understood in terms of the internal OH reactivity provided by O₃. When internal OH reactivity is larger or similar to external OH reactivity, the chemistry is resilient to the external perturbation. However when external OH reactivity is much larger than internal OH reactivity, the recycling of OH via HO₂ + O₃ → OH + O₂ is too slow and major OH suppression is observed. As many OFR studies have been conducted in that regime, this finding has important implications for their interpretation. Use of measurements under low external OH reactivity to estimate OH exposure at high external OH reactivity can lead to errors exceeding 1 order of magnitude.

We derived two estimation equations for OH exposure in OFR254 over a very wide range of H₂O concentration, UV photon flux, external OH reactivity, and initial O₃ concentration. The input parameters of the two equations are H₂O, UV, OHR_{ext}, and initial O₃ concentration, and of O₃ loss ratio, external OH reactivity, and initial O₃ concentration, respectively. The latter equation avoids the need to estimate effective UV photon flux that is difficult to determine accurately, and also more closely captures the model-calculated OH exposure (mean absolute value of the relative deviation: 10 % vs. 15 %). Thus, measuring O₃ concentrations at both OFR's entrance and the exit is recommended for more accurate exposure estimation. The method demonstrated here can be used to derive modified estimation equations under conditions different than those considered here, e.g., with lower HO₂ recycling or different evolution of OHR_{ext} in the reactor than when using SO₂ as the reactant, or when using different UV sources.

As our study is systematic and covers a very large range of conditions, it not only provides more reliable insights into the gas-phase chemistry in OFRs, but also shows that OFR radical chemistry is controllable by regulating experimental conditions and predictable by modeling. Our findings will help the experimental design and the interpretation of results in future OFR studies, which would benefit OFR users in atmospheric research, e.g., SOA formation and aging, as well as those employing OFRs for other purposes, e.g., pollution scrubbing. Our results may also contribute to the design of OFRs with better properties in the future.

Appendix A: Glossary.

Table A1.

OFR	oxidation flow reactor
OFR185	oxidation flow reactor using both 185 and 254 nm light
OFR254	oxidation flow reactor using 254 nm light only
OFR254-X	OFR254 with X ppm O ₃ initially injected
OH _{exp}	OH exposure
H ₂ O	water mixing ratio
UV	UV light intensity
O ₃	O ₃ concentration
OHR	OH reactivity
OHR _{tot}	total OH reactivity
OHR _{int}	internal OH reactivity (due to O ₃ , HO ₂ , OH, and H ₂ O ₂)
OHR _{ext}	external OH reactivity
OHR _{O₃}	OH reactivity from O ₃ only
VOC	volatile organic compound
SOA	secondary organic aerosol
RTD	residence time distribution
OH _{exp,PF}	OH exposure in the plug-flow model
OH _{exp,RTD} ^{MATH}	OH exposure calculated from direct integration in the models with residence time distribution
OH _{exp,LB} ^{MATH}	OH exposure calculated from direct integration in the models with the Lambe et al. (2011a) residence time distribution
OH _{exp,RTD} ^{SO₂}	OH exposure estimated from SO ₂ decay in the models with residence time distribution
OH _{exp,LB} ^{SO₂}	OH exposure estimated from SO ₂ decay in the models with the Lambe et al. (2011a) residence time distribution
rOH _{exp}	Ratio of remaining OH after suppression
O _{3,in}	O ₃ concentration at the reactor entrance
O _{3,out}	O ₃ concentration at the reactor exit
rO ₃	ratio of O _{3,out} to O _{3,in}

The Supplement related to this article is available online at doi:10.5194/amt-8-4863-2015-supplement.

Acknowledgements. We thank the PAM user community as well as Weiwei Hu, and Amber Ortega for useful discussions, and Andrew Lambe and Daniel Tkacik for providing some OFR experimental data. This research was partially supported by CARB 11-305, DOE (BER/ASR program) DE-SC0011105, and NSF AGS-1243354 & AGS-1360834. R. Li and B. B. Palm acknowledge CIRES Graduate Student Fellowships. B. B. Palm is grateful for a graduate fellowship from US EPA STAR (FP-91761701-0). This manuscript has not been reviewed by EPA and thus no endorsement should be inferred.

Edited by: D. Heard

References

- Andreozzi, R., Caprio, V., Insola, A., and Marotta, R.: Advanced oxidation processes (AOP) for water purification and recovery, *Catal. Today*, 53, 51–59, doi:10.1016/S0920-5861(99)00102-9, 1999.
- Bahreini, R., Middlebrook, A. M., Brock, C. A., de Gouw, J. A., McKeen, S. A., Williams, L. R., Daumit, K. E., Lambe, A. T., Massoli, P., Canagaratna, M. R., Ahmadov, R., Carrasquillo, A. J., Cross, E. S., Ervens, B., Holloway, J. S., Hunter, J. F., Onasch, T. B., Pollack, I. B., Roberts, J. M., Ryerson, T. B., Warneke, C., Davidovits, P., Worsnop, D. R., and Kroll, J. H.: Mass spectral analysis of organic aerosol formed downwind of the Deepwater Horizon oil spill: field studies and laboratory confirmations., *Environ. Sci. Technol.*, 46, 8025–34, doi:10.1021/es301691k, 2012.
- BIPM, IEC, IFCC, ILAC, ISO, IUPAC and IUPAPOIML: JCGM 101: 2008 Evaluation of measurement data – Supplement 1 to the “ Guide to the expression of uncertainty in measurement ” – Propagation of distributions using a Monte Carlo method, available at: http://www.bipm.org/utis/common/documents/jcgm/JCGM_101_2008_E.pdf, 2008.
- Bonn, B., Bourtsoukidis, E., Sun, T. S., Bingemer, H., Rondo, L., Javed, U., Li, J., Axinte, R., Li, X., Brauers, T., Sonderfeld, H., Koppmann, R., Sogachev, A., Jacobi, S., and Spracklen, D. V.: The link between atmospheric radicals and newly formed particles at a spruce forest site in Germany, *Atmos. Chem. Phys.*, 14, 10823–10843, doi:10.5194/acp-14-10823-2014, 2014.
- Borbon, A., Gilman, J. B., Kuster, W. C., Grand, N., Chevaillier, S., Colomb, A., Dolgorouky, C., Gros, V., Lopez, M., Sarda-Esteve, R., Holloway, J., Stutz, J., Petetin, H., McKeen, S., Beekmann, M., Warneke, C., Parrish, D. D., and De Gouw, J. A.: Emission ratios of anthropogenic volatile organic compounds in northern mid-latitude megacities: Observations versus emission inventories in Los Angeles and Paris, *J. Geophys. Res. Atmos.*, 118, 2041–2057, doi:10.1002/jgrd.50059, 2013.
- Carlton, A. G., Wiedinmyer, C., and Kroll, J. H.: A review of Secondary Organic Aerosol (SOA) formation from isoprene, *Atmos. Chem. Phys.*, 9, 4987–5005, doi:10.5194/acp-9-4987-2009, 2009.
- Carter, W. P. L., Cocker, D. R., Fitz, D. R., Malkina, I. L., Bumiller, K., Sauer, C. G., Pisano, J. T., Bufalino, C., and Song, C.: A new environmental chamber for evaluation of gas-phase chemical mechanisms and secondary aerosol formation, *Atmos. Environ.*, 39, 7768–7788, doi:10.1016/j.atmosenv.2005.08.040, 2005.
- Cocker, D. R., Flagan, R. C., and Seinfeld, J. H.: State-of-the-art chamber facility for studying atmospheric aerosol chemistry., *Environ. Sci. Technol.*, 35, 2594–601, 2001.
- Cubison, M. J., Ortega, A. M., Hayes, P. L., Farmer, D. K., Day, D., Lechner, M. J., Brune, W. H., Apel, E., Diskin, G. S., Fisher, J. A., Fuelberg, H. E., Hecobian, A., Knapp, D. J., Mikoviny, T., Riemer, D., Sachse, G. W., Sessions, W., Weber, R. J., Weinheimer, A. J., Wisthaler, A., and Jimenez, J. L.: Effects of aging on organic aerosol from open biomass burning smoke in aircraft and laboratory studies, *Atmos. Chem. Phys.*, 11, 12049–12064, doi:10.5194/acp-11-12049-2011, 2011.
- Danet, A. F., Bratu, M.-C., Radulescu, M.-C., and Bratu, A.: Portable minianalyzer based on cold vapor atomic absorption spectrometry at 184.9nm for atmospheric mercury determination, *Sensors Actuators B Chem.*, 137, 12–16, doi:10.1016/j.snb.2008.12.065, 2009.
- Environment Canada: National ambient levels of ozone, available at: <https://www.ec.gc.ca/indicateurs-indicators/default.asp?lang=en&n=9EBBCA88-1#01> (last access: April 2015), 2014.
- Gans, B., Peng, Z., Carrasco, N., Gauyacq, D., Lebonnois, S., and Pernot, P.: Impact of a new wavelength-dependent representation of methane photolysis branching ratios on the modeling of Titan’s atmospheric photochemistry, *Icarus*, 223, 330–343, doi:10.1016/j.icarus.2012.11.024, 2013.
- George, I. J., Vlasenko, A., Slowik, J. G., Broekhuizen, K., and Abbatt, J. P. D.: Heterogeneous oxidation of saturated organic aerosols by hydroxyl radicals: uptake kinetics, condensed-phase products, and particle size change, *Atmos. Chem. Phys.*, 7, 4187–4201, doi:10.5194/acp-7-4187-2007, 2007.
- Hallquist, M., Wenger, J. C., Baltensperger, U., Rudich, Y., Simpson, D., Claeys, M., Dommen, J., Donahue, N. M., George, C., Goldstein, A. H., Hamilton, J. F., Herrmann, H., Hoffmann, T., Iinuma, Y., Jang, M., Jenkin, M. E., Jimenez, J. L., Kiendler-Scharr, A., Maenhaut, W., McFiggans, G., Mentel, Th. F., Monod, A., Prévôt, A. S. H., Seinfeld, J. H., Surratt, J. D., Szmigielski, R., and Wildt, J.: The formation, properties and impact of secondary organic aerosol: current and emerging issues, *Atmos. Chem. Phys.*, 9, 5155–5236, doi:10.5194/acp-9-5155-2009, 2009.
- Hanna, S. R., Lu, Z., Frey, H. C., Wheeler, N., Vukovich, J., Arunachalam, S., Fernau, M., and Hansen, D. A.: Uncertainties in predicted ozone concentrations due to input uncertainties for the UAM-V photochemical grid model applied to the July 1995 OTAG domain, *Atmos. Environ.*, 35, 891–903, doi:10.1016/S1352-2310(00)00367-8, 2001.
- Hébrard, E., Dobrijevic, M., Bénilan, Y., and Raulin, F.: Photochemical kinetics uncertainties in modeling Titan’s atmosphere: A review, *J. Photochem. Photobiol. C Photochem. Rev.*, 7, 211–230, doi:10.1016/j.jphotochemrev.2006.12.004, 2006.
- Hébrard, E., Dobrijevic, M., Pernot, P., Carrasco, N., Bergeat, A., Hickson, K. M., Canosa, A., Le Picard, S. D., and Sims, I. R.: How measurements of rate coefficients at low temperature increase the predictivity of photochemical models of

- Titan's atmosphere., *J. Phys. Chem. A*, 113, 11227–11237, doi:10.1021/jp905524e, 2009.
- Johnson, M. S., Nilsson, E. J. K., Svensson, E. A., and Langer, S.: Gas-phase advanced oxidation for effective, efficient in situ control of pollution., *Environ. Sci. Technol.*, 48, 8768–8776, doi:10.1021/es5012687, 2014.
- Kang, E., Root, M. J., Toohey, D. W., and Brune, W. H.: Introducing the concept of Potential Aerosol Mass (PAM), *Atmos. Chem. Phys.*, 7, 5727–5744, doi:10.5194/acp-7-5727-2007, 2007.
- Kang, E., Toohey, D. W., and Brune, W. H.: Dependence of SOA oxidation on organic aerosol mass concentration and OH exposure: experimental PAM chamber studies, *Atmos. Chem. Phys.*, 11, 1837–1852, doi:10.5194/acp-11-1837-2011, 2011.
- Krechmer, J. E., Coggon, M. M., Massoli, P., Nguyen, T. B., Crouse, J. D., Hu, W., Day, D. A., Tyndall, G. S., Henze, D. K., Rivera-Rios, J. C., Nowak, J. B., Kimmel, J. R., Mauldin, R. L., Stark, H., Jayne, J. T., Sipilä, M., Junninen, H., Clair, J. M. St., Zhang, X., Feiner, P. A., Zhang, L., Miller, D. O., Brune, W. H., Keutsch, F. N., Wennberg, P. O., Seinfeld, J. H., Worsnop, D. R., Jimenez, J. L., and Canagaratna, M. R.: Formation of Low Volatility Organic Compounds and Secondary Organic Aerosol from Isoprene Hydroxyhydroperoxide Low-NO Oxidation, *Environ. Sci. Technol.*, 49, 10330–10339, doi:10.1021/acs.est.5b02031, 2015.
- Kumata, K., Itoh, U., Toyoshima, Y., Tanaka, N., Anzai, H., and Matsuda, A.: Photochemical vapor deposition of hydrogenated amorphous silicon films from disilane and trisilane using a low pressure mercury lamp, *Appl. Phys. Lett.*, 48, 1380, doi:10.1063/1.96915, 1986.
- Lambe, A. T.: Interactive comment on “Comparison of secondary organic aerosol formed with an aerosol flow reactor and environmental reaction chambers: effect of oxidant concentration, exposure time and seed particles on chemical composition and yield” by A. T. Lambe et al., *Atmos. Chem. Phys. Discuss.*, 14, C12169, available at: www.atmos-chem-phys-discuss.net/14/C12169/2015/, 2015.
- Lambe, A. T., Ahern, A. T., Williams, L. R., Slowik, J. G., Wong, J. P. S., Abbatt, J. P. D., Brune, W. H., Ng, N. L., Wright, J. P., Croasdale, D. R., Worsnop, D. R., Davidovits, P., and Onasch, T. B.: Characterization of aerosol photooxidation flow reactors: heterogeneous oxidation, secondary organic aerosol formation and cloud condensation nuclei activity measurements, *Atmos. Meas. Tech.*, 4, 445–461, doi:10.5194/amt-4-445-2011, 2011a.
- Lambe, A. T., Onasch, T. B., Massoli, P., Croasdale, D. R., Wright, J. P., Ahern, A. T., Williams, L. R., Worsnop, D. R., Brune, W. H., and Davidovits, P.: Laboratory studies of the chemical composition and cloud condensation nuclei (CCN) activity of secondary organic aerosol (SOA) and oxidized primary organic aerosol (OPOA), *Atmos. Chem. Phys.*, 11, 8913–8928, doi:10.5194/acp-11-8913-2011, 2011b.
- Lambe, A. T., Onasch, T. B., Croasdale, D. R., Wright, J. P., Martin, A. T., Franklin, J. P., Massoli, P., Kroll, J. H., Canagaratna, M. R., Brune, W. H., Worsnop, D. R., and Davidovits, P.: Transitions from functionalization to fragmentation reactions of laboratory secondary organic aerosol (SOA) generated from the OH oxidation of alkane precursors., *Environ. Sci. Technol.*, 46, 5430–5437, doi:10.1021/es300274t, 2012.
- Lambe, A. T., Cappa, C. D., Massoli, P., Onasch, T. B., Forestieri, S. D., Martin, A. T., Cummings, M. J., Croasdale, D. R., Brune, W. H., Worsnop, D. R., and Davidovits, P.: Relationship between oxidation level and optical properties of secondary organic aerosol., *Environ. Sci. Technol.*, 47, 6349–6357, doi:10.1021/es401043j, 2013.
- Lambe, A. T., Chhabra, P. S., Onasch, T. B., Brune, W. H., Hunter, J. F., Kroll, J. H., Cummings, M. J., Brogan, J. F., Parmar, Y., Worsnop, D. R., Kolb, C. E., and Davidovits, P.: Effect of oxidant concentration, exposure time, and seed particles on secondary organic aerosol chemical composition and yield, *Atmos. Chem. Phys.*, 15, 3063–3075, doi:10.5194/acp-15-3063-2015, 2015.
- Legrini, O., Oliveros, E., and Braun, A. M.: Photochemical processes for water treatment, *Chem. Rev.*, 93, 671–698, doi:10.1021/cr00018a003, 1993.
- Levy II, H.: Normal atmosphere: large radical and formaldehyde concentrations predicted, *Science*, 173, 141–143, doi:10.1126/science.173.3992.141, 1971.
- Li, R., Palm, B. B., Borbon, A., Graus, M., Warneke, C., Ortega, A. M., Day, D. A., Brune, W. H., Jimenez, J. L., and de Gouw, J. A.: Laboratory studies on secondary organic aerosol formation from crude oil vapors, *Environ. Sci. Technol.*, 47, 12566–12574, doi:10.1021/es402265y, 2013.
- Li, R., Palm, B. B., Ortega, A. M., Hu, W., Peng, Z., Day, D. A., Knote, C., Brune, W. H., de Gouw, J., and Jimenez, J. L.: Modeling the radical chemistry in an Oxidation Flow Reactor (OFR): radical formation and recycling, sensitivities, and OH exposure estimation equation, *J. Phys. Chem. A*, 119, 4418–4432, doi:10.1021/jp509534k, 2015.
- Liu, P. F., Abdelmalki, N., Hung, H.-M., Wang, Y., Brune, W. H., and Martin, S. T.: Ultraviolet and visible complex refractive indices of secondary organic material produced by photooxidation of the aromatic compounds toluene and *m*-xylene, *Atmos. Chem. Phys.*, 15, 1435–1446, doi:10.5194/acp-15-1435-2015, 2015.
- Liu, Y. J., Herdinger-Blatt, I., McKinney, K. A., and Martin, S. T.: Production of methyl vinyl ketone and methacrolein via the hydroperoxyl pathway of isoprene oxidation, *Atmos. Chem. Phys.*, 13, 5715–5730, doi:10.5194/acp-13-5715-2013, 2013.
- Ma, X. and Xia, Y.: Pinpointing double bonds in lipids by Paternò-Büchi reactions and mass spectrometry, *Angew. Chem. Int. Ed. Engl.*, 53, 2592–2596, doi:10.1002/anie.201310699, 2014.
- Mao, J., Ren, X., Brune, W. H., Olson, J. R., Crawford, J. H., Fried, A., Huey, L. G., Cohen, R. C., Heikes, B., Singh, H. B., Blake, D. R., Sachse, G. W., Diskin, G. S., Hall, S. R., and Shetter, R. E.: Airborne measurement of OH reactivity during INTEX-B, *Atmos. Chem. Phys.*, 9, 163–173, doi:10.5194/acp-9-163-2009, 2009.
- Massoli, P., Lambe, A. T., Ahern, A. T., Williams, L. R., Ehn, M., Mikkilä, J., Canagaratna, M. R., Brune, W. H., Onasch, T. B., Jayne, J. T., Petäjä, T., Kulmala, M., Laaksonen, A., Kolb, C. E., Davidovits, P., and Worsnop, D. R.: Relationship between aerosol oxidation level and hygroscopic properties of laboratory generated secondary organic aerosol (SOA) particles, *Geophys. Res. Lett.*, 37, L24801, doi:10.1029/2010GL045258, 2010.
- Mory, M.: *Fluid Mechanics for Chemical Engineering*, John Wiley & Sons, Inc., Hoboken, NJ USA, 422 pp., 2013.
- Ono, R., Nakagawa, Y., Tokumitsu, Y., Matsumoto, H., and Oda, T.: Effect of humidity on the production of ozone and other radicals by low-pressure mercury lamps, *J. Photochem. Photobiol. A Chem.*, 274, 13–19, doi:10.1016/j.jphotochem.2013.09.012, 2014.

- Ortega, A. M., Day, D. A., Cubison, M. J., Brune, W. H., Bon, D., de Gouw, J. A., and Jimenez, J. L.: Secondary organic aerosol formation and primary organic aerosol oxidation from biomass-burning smoke in a flow reactor during FLAME-3, *Atmos. Chem. Phys.*, 13, 11551–11571, doi:10.5194/acp-13-11551-2013, 2013.
- Ortega, A. M., Hayes, P. L., Peng, Z., Palm, B. B., Hu, W., Day, D. A., Li, R., Cubison, M. J., Brune, W. H., Graus, M., Warneke, C., Gilman, J. B., Kuster, W. C., de Gouw, J. A., and Jimenez, J. L.: Real-time measurements of secondary organic aerosol formation and aging from ambient air in an oxidation flow reactor in the Los Angeles area, *Atmos. Chem. Phys. Discuss.*, 15, 21907–21958, doi:10.5194/acpd-15-21907-2015, 2015.
- Palm, B. B., Campuzano-Jost, P., Ortega, A. M., Day, D. A., Kaser, L., Jud, W., Karl, T., Hansel, A., Hunter, J. F., Cross, E. S., Kroll, J. H., Peng, Z., Brune, W. H., and Jimenez, J. L.: In situ secondary organic aerosol formation from ambient pine forest air using an oxidation flow reactor, *Atmos. Chem. Phys. Discuss.*, 15, 30409–30471, doi:10.5194/acpd-15-30409-2015, 2015.
- Paulot, F., Crounse, J. D., Kjaergaard, H. G., Kurten, A., St. Clair, J. M., Seinfeld, J. H., and Wennberg, P. O.: Unexpected Epoxide Formation in the Gas-Phase Photooxidation of Isoprene, *Science*, 80, 325, 730–733, doi:10.1126/science.1172910, 2009.
- Peng, Z., Cailliez, F., Dobrijevic, M., and Pernot, P.: Null Variance Altitudes for the photolysis rate constants of species with barometric distribution: Illustration on Titan upper atmosphere modeling, *Icarus*, 218, 950–955, doi:10.1016/j.icarus.2012.02.006, 2012.
- Peng, Z., Carrasco, N., and Pernot, P.: Modeling of synchrotron-based laboratory simulations of Titan's ionospheric photochemistry, *GeoResJ*, 1–2, 33–53, doi:10.1016/j.grj.2014.03.002, 2014.
- Peng, Z., Day, D. A., Ortega, A. M., Palm, B. B., Hu, W. W., Stark, H., Li, R., Tsigaridis, K., Brune, W. H., and Jimenez, J. L.: Non-OH chemistry in oxidation flow reactors for the study of atmospheric chemistry systematically examined by modeling, *Atmos. Chem. Phys. Discuss.*, 15, 23543–23586, doi:10.5194/acpd-15-23543-2015, 2015.
- Peng, Z., Dobrijevic, M., Hébrard, E., Carrasco, N., and Pernot, P.: Photochemical modeling of Titan atmosphere at the “10 percent uncertainty horizon,” *Faraday Discuss.*, 147, 137, doi:10.1039/c003366a, 2010.
- Platt, S. M., El Haddad, I., Zardini, A. A., Clairotte, M., Astorga, C., Wolf, R., Slowik, J. G., Temime-Roussel, B., Marchand, N., Ježek, I., Drinovec, L., Mocnik, G., Möhler, O., Richter, R., Barmet, P., Bianchi, F., Baltensperger, U., and Prévôt, A. S. H.: Secondary organic aerosol formation from gasoline vehicle emissions in a new mobile environmental reaction chamber, *Atmos. Chem. Phys.*, 13, 9141–9158, doi:10.5194/acp-13-9141-2013, 2013.
- Presto, A. A., Huff Hartz, K. E., and Donahue, N. M.: Secondary Organic Aerosol Production from Terpene Ozonolysis. 1. Effect of UV Radiation, *Environ. Sci. Technol.*, 39, 7036–7045, doi:10.1021/es050174m, 2005.
- Saltelli, A., Ratto, M., Tarantola, S., and Campolongo, F.: Sensitivity analysis for chemical models, *Chem. Rev.*, 105, 2811–2828, doi:10.1021/cr040659d, 2005.
- Sander, S. P., Friedl, R. R., Barker, J. R., Golden, D. M., Kurylo, M. J., Wine, P. H., Abbatt, J. P. D., Burkholder, J. B., Kolb, C. E., Moortgat, G. K., Huie, R. E., and Orkin, V. L.: Chemical Kinetics and Photochemical Data for Use in Atmospheric Studies Evaluation Number 17, 2011.
- Saukko, E., Lambe, A. T., Massoli, P., Koop, T., Wright, J. P., Croasdale, D. R., Pedernera, D. A., Onasch, T. B., Laaksonen, A., Davidovits, P., Worsnop, D. R., and Virtanen, A.: Humidity-dependent phase state of SOA particles from biogenic and anthropogenic precursors, *Atmos. Chem. Phys.*, 12, 7517–7529, doi:10.5194/acp-12-7517-2012, 2012.
- Seakins, P. W.: A brief review of the use of environmental chambers for gas phase studies of kinetics, chemical mechanisms and characterisation of field instruments, *EPJ Web Conf.*, 9, 143–163, doi:10.1051/epjconf/201009012, 2010.
- Stone, D., Whalley, L. K., and Heard, D. E.: Tropospheric OH and HO₂ radicals: field measurements and model comparisons, *Chem. Soc. Rev.*, 41, 6348–6404, doi:10.1039/c2cs35140d, 2012.
- Tkacik, D. S., Lambe, A. T., Jathar, S., Li, X., Presto, A. A., Zhao, Y., Blake, D., Meinardi, S., Jayne, J. T., Croteau, P. L., and Robinson, A. L.: Secondary Organic Aerosol Formation from in-Use Motor Vehicle Emissions Using a Potential Aerosol Mass Reactor, *Environ. Sci. Technol.*, 48, 11235–11242, doi:10.1021/es502239v, 2014.
- Volkamer, R., Jimenez, J. L., San Martini, F., Dzepina, K., Zhang, Q., Salcedo, D., Molina, L. T., Worsnop, D. R., and Molina, M. J.: Secondary organic aerosol formation from anthropogenic air pollution: Rapid and higher than expected, *Geophys. Res. Lett.*, 33, L17811, doi:10.1029/2006GL026899, 2006.
- Wakelam, V., Smith, I. W. M., Herbst, E., Troe, J., Geppert, W., Linnartz, H., Öberg, K., Roueff, E., Agúndez, M., Pernot, P., Cuppen, H. M., Loison, J. C., and Talbi, D.: Reaction Networks for Interstellar Chemical Modelling: Improvements and Challenges, *Space Sci. Rev.*, 156, 13–72, doi:10.1007/s11214-010-9712-5, 2010.
- Wang, B., Lambe, A. T., Massoli, P., Onasch, T. B., Davidovits, P., Worsnop, D. R., and Knopf, D. A.: The deposition ice nucleation and immersion freezing potential of amorphous secondary organic aerosol: Pathways for ice and mixed-phase cloud formation, *J. Geophys. Res.*, 117, D16209, doi:10.1029/2012JD018063, 2012.
- Wang, J., Doussin, J. F., Perrier, S., Perraudin, E., Katrib, Y., Pangui, E., and Picquet-Varrault, B.: Design of a new multi-phase experimental simulation chamber for atmospheric photochemical aerosol and cloud chemistry research, *Atmos. Meas. Tech.*, 4, 2465–2494, doi:10.5194/amt-4-2465-2011, 2011.
- Witte, K. J., Burkhard, P., and Lüthi, H. R.: Low-pressure mercury lamp pumped atomic iodine laser of high efficiency, *Opt. Commun.*, 28, 202–206, doi:10.1016/0030-4018(79)90268-2, 1979.
- Ye, J., Shang, J., Li, Q., Xu, W., Liu, J., Feng, X., and Zhu, T.: The use of vacuum ultraviolet irradiation to oxidize SO₂ and NO_x for simultaneous desulfurization and denitrification, *J. Hazard. Mater.*, 271, 89–97, doi:10.1016/j.jhazmat.2014.02.011, 2014.